Supporting information

Polymorphism of derivatives of tert-butyl substituted acridan and perfluorobiphenyl as sky-blue OLED emitters exhibiting aggregation induced thermally activated delayed fluorescence

Iryna Hladka[1], Dmytro Volyniuk[1], Oleksandr Bezvikonnyi[1], Vasyl Kinzhybalo[2], Tamara Bednarchuk[2], Yan Danyliv[1], Roman Lytvyn[1,3], Algirdas Lazauskas[4], Juozas V. Grazulevicius[1,]*

[1]Department of Polymer Chemistry and Technology, Kaunas University of Technology, Radvilenu pl. 19, LT-50254, Kaunas, Lithuania; e-mail: juozas.grazulevicius@ktu.lt.

[2]Institute of Low Temperature and Structure Research, Polish Academy of Sciences, Okólna 2, 50-422 Wrocław, Poland

[3]Department of Organic Chemistry, Ivan Franko National University of Lviv, Kyryla i Mefodia St. 6, 79005 Lviv, Ukraine.

[4]Institute of Materials Science, Kaunas University of Technology, K. Baršausko St. 59, LT51423 Kaunas, Lithuania

[*] Corresponding author. E-mail address: juozas.grazulevicius@ktu.lt (Juozas Vidas Grazulevicius)

Instrumentation

^{1}H, ^{13}C and ^{19}F nuclear magnetic resonance (NMR) spectra of the solutions in deuterated chloroform ($CDCl_3$) were obtained using Bruker DRX 400 spectrometer (400 MHz (^{1}H), 100 MHz (^{13}C), 375 MHz (^{19}F)). Chemical shifts (δ) are reported in ppm referenced to tetramethylsilane (TMS). Mass spectra were obtained by the electrospray ionization mass spectrometry (ESI-MS) method on Esquire-LC 00084 mass spectrometer. Elemental analysis data were obtained on a EuroEA Elemental Analyser. For X-ray crystallography analysis diffraction data were collected on a Bruker-Nonius KappaCCD single diffractometer using graphite monochromated Mo-Kα radiation (λ = 0.71073 Å). The crystal structure was solved by direct method [SIR-97] and refined by full-matrix least squares [SHELXL-97].

The intensity data for compounds **PFBP-1a**, **PFBP-1b** and **PFBP-2b_crystalB** were collected at 100 K on an Oxford Diffraction Xcalibur diffractometer equipped with graphite-monochromated Mo Ka radiation (λ = 0.71073 Å). The instrument was equipped with an Oxford Cryosystems 800 series cryocooler. Data collection and reduction were made using CrysAlisCCD and CrysAlis RED programs (Rigaku, 2015). The crystallographic measurement for compound **PFBP-2b_crystalA** was performed at 295 K on a XtaLAB Mini (ROW) diffractometer. A numerical absorption correction based on the shape of the crystals was performed. The crystal structures were solved by direct methods and all non-hydrogen atoms were refined anisotropically with full-matrix least-squares techniques on F^2 by SHELXL with the following graphical user interfaces of OLEX^2 (Sheldrick, 2015; Dolomanov *et al.*, 2009). For all structures H-atom parameters were constrained. In compound **PFBP-2a_crystalA** one of two *tert*-butyl groups is disordered over two positions with site occupancies of 0.645(15) and 0.355(15). In order to avoid the distortion of the disordered *tert*-butyl group, SHELXL (SADI, DELU and SIMU) instructions were used. In compound **PFBP-2a_crystalB** both *tert*-butyl functional groups are disordered over two sets of sites, with occupancy ratio of 0.538(5):0.462(5) and 0.937(3):0.063(3). The second disordered *tert*-butyl group was refined with distance and angles restraints, and the minor component atoms C33-C35 were refined isotropically.

Details on the single crystal X-ray data collection, reduction and structure parameters for all compounds are given in Tables S2-S5.

The crystallographic nature of **PFBP-1a**, **PFBP-1b**, **PFBP-2a and PFBP-2b** powders was determined using D8 Discover X-ray diffractometer (Bruker AXS GmbH) with Cu K_α (λ= 1.54 Å) X-ray source. Parallel beam geometry with 60 mm Göbel mirror (i.e. X-ray mirror on a high precision parabolic surface) was used. This configuration enables transforming the divergent incident X-ray beam from a line focus of the X-ray tube into a parallel beam that is free of K_β radiation. Primary side also had a Soller slit with an axial divergence of 2.5 º and divergence slit of 1.0 mm. The secondary side had a LYNXEYE (0D mode) detector with an opening angle of 2.160 º and slit opening of 6.0 mm. X-ray generator voltage and current was 40.0 kV and 40 mA, respectively. Coupled 2θ/θ scans were performed in the range of 4.0-135.0 º with a step size of 0.065 º, time per step of 19.2 s and auto-repeat function enabled. Processing of the resultant diffractograms was performed with DIFFRAC.EVA software. For the X-ray diffraction measurements at grazing incidence (XRDGI) the divergence slit of 0.6 mm was used on the primary side. The XRDGI scans for thin films of **PFBP-1a**, **PFBP-1a:TCz1**, **PFBP-1b, PFBP-1b:TCz1**, **PFBP-2a**, **PFBP-2a:TCz1**, **PFBP-2b** and **PFBP-2b:TCz1** were performed at incidence angle of 1.50 º, in the range of 4.-134.0 º with a step size of 0.065 º, time per step of 19.2 s and auto-repeat function enabled. Macromolecular orientation texture analysis of **PFBP-2a** (sample prepared using drop casting method) was performed to describe the variation in the pole density (i.e. determined by the intensity of diffracted X-ray beam) with pole orientation for crystalline component reflection at 7.21º in 2θ. Data were collected using a standard mode (unlocked coupled) with 5º of δ measured for full circle 0-360 incr. 5º in Phi (φ) and 0-10 incr. 10º in Psi (ψ) range. Measured data were corrected for background scattering and the defocusing of the beam using Diffrac^{plus} MULTEX 3 software package.

Surface morphology of **PFBP-1a**, **PFBP-1a:TCz1**, **PFBP-1b, PFBP-1b:TCz1**, **PFBP-2a**, **PFBP-2a:TCz1**, **PFBP-2b** and **PFBP-2b:TCz1** thin films was investigated using atomic force microscopy (AFM). AFM experiments were carried out in air at room temperature using a NanoWizardIII atomic force microscope (JPK Instruments), while data was analysed using SurfaceXplorer and JPKSPM Data Processing software. The AFM images were collected using a V-shaped silicon cantilever (spring constant of 3 N/m, tip curvature radius of 10.0 nm and the cone angle of 20º) operating in a contact mode.

Theoretical calculations of the **PFBP** derivatives were performed using density-functional theory via Spartan'14 software package. UV/Vis spectra of 10^{-4} M solutions of the compounds were recorded in quartz cells using Perkin Elmer Lambda 35 spectrometer. Photoluminescence (PL) spectra of 10^{-5} M solutions of the compounds were recorded using Edinburgh Instruments' FLS980 Fluorescence Spectrometer. Thin solid films for recording UV/Vis and PL spectra were prepared by spin-coating technique utilizing SPS-Europe Spin150 Spin processor using 2.5 mg/ml solutions of the compounds in THF on the pre-cleaned quartz substrates. Photoluminescence quantum yields of the solutions and oh the solid films were determined using the integrated sphere (Edinburgh Instruments) coupled to the FLS980 spectrometer, calibrated with two standards: quinine sulphate in 0.1 H_2SO_4 and rhodamine 6G in ethanol).[1]

Differential scanning calorimetry (DSC) measurements were done with a TA Instruments "DSC Q100" calorimeter. The samples were heated at a scan rate of 10 °C/min under nitrogen atmosphere. Thermogravimetric analysis (TGA) was performed on a "Mettler TGA/SDTA851e/LF/1100" at a heating rate of 20 °C/min under nitrogen atmosphere. Electrochemical measurements were done using μAutolab Type III (EcoChemie, Netherlands) potentiostat, glassy carbon electrode (diam. 2 mm), platinum coil and silver wire as working, auxiliary and reference electrode, respectively and the scan rate of 2.5 mV/s with concentration of compounds 1.0×10^{-4} mol/dm^3. Potentials are referenced with respect to ferrocene (Fc), which was used as the internal standard. Cyclic voltammetry (CV) experiments were conducted in the dry solvent solution containing 0.1 M tetrabutylammonium hexafluorophosphate ($TBAPF_6$) as the electrolyte at room temperature under nitrogen atmosphere. For all synthesized compounds, measurements were done in DMF solution. Deaeration of the solution was achieved by a nitrogen bubbling for about 10 min before measurement.

Photoelectron emission spectra for vacuum deposited layers of the studied compounds were recorded to obtain the solid-state ionization potentials (Ip_{PE}) of the compounds as reported previously.[2,3] Fluorine doped tin oxide (FTO) coated glass slides were used as substrates for the preparation of samples for photoelectron emission spectrometry. The layers of the compounds were fabricated by thermal vacuum evaporation onto the substrates. Photoelectron emission spectra were recorded in air using ASBN-D130-CM deep UV deuterium light source, CM110 1/8m monochromator and 6517B Keithley electrometer.

Device fabrications

The following devices were fabricated and characterized as it was described earlier.[4]

Device A: ITO/MoO_3(4nm)/NPB(45nm)/ **PFBP-1b**:mCP(10-90%,30nm)/TPBi(45nm)/Ca/Al

Device B: ITO/MoO_3(4nm)/NPB(70nm)/ **PFBP-2a**:TCz1(15-85%,20nm)/TPBi(30nm)/Ca/Al

Device C: ITO/MoO_3(4nm)/NPB(45nm)/ **PFBP-2b** (30nm)/TPBi(50nm)/Ca/Al

Device D: ITO/MoO_3(4nm)/NPB(45nm)/ **PFBP-2b**:TCz1(15-85%,30nm)/TPBi(45nm)/Ca/Al

Materials

The starting compounds i.e. decafluorobiphenyl and potassium hydroxide (KOH) were purchased from Sigma-Aldrich; 9,9-dimethyl-9,10-dihydro-acridine and 2,7-di-*tert*-butyl-9,9-dimethyl-9,10-dihydro-acridine were obtained from Center for physical sciences and technology (Vilnius) and used as received.

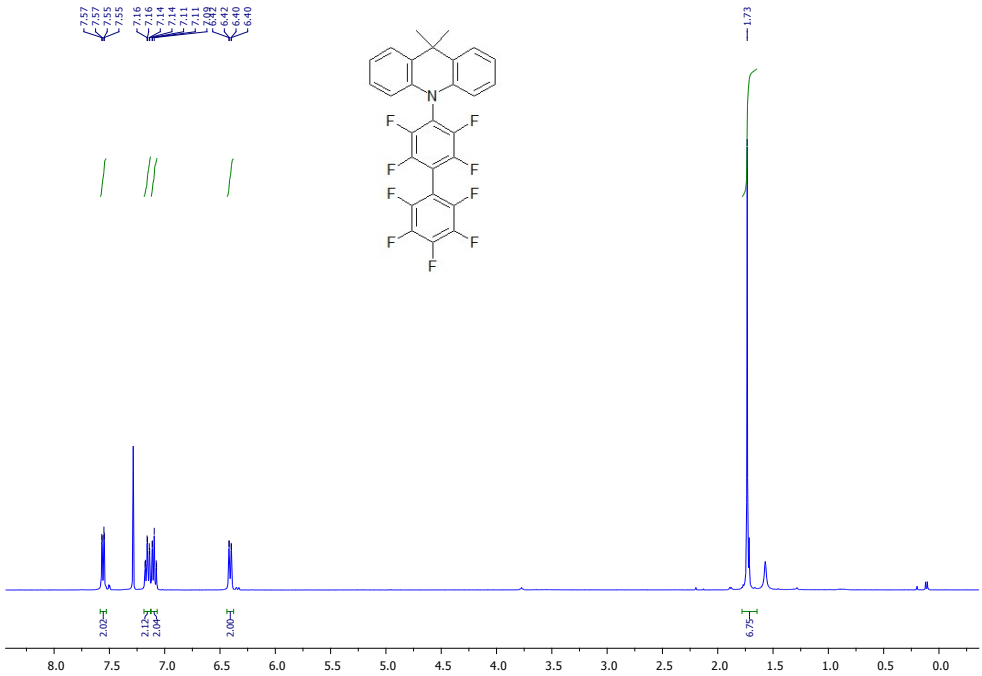

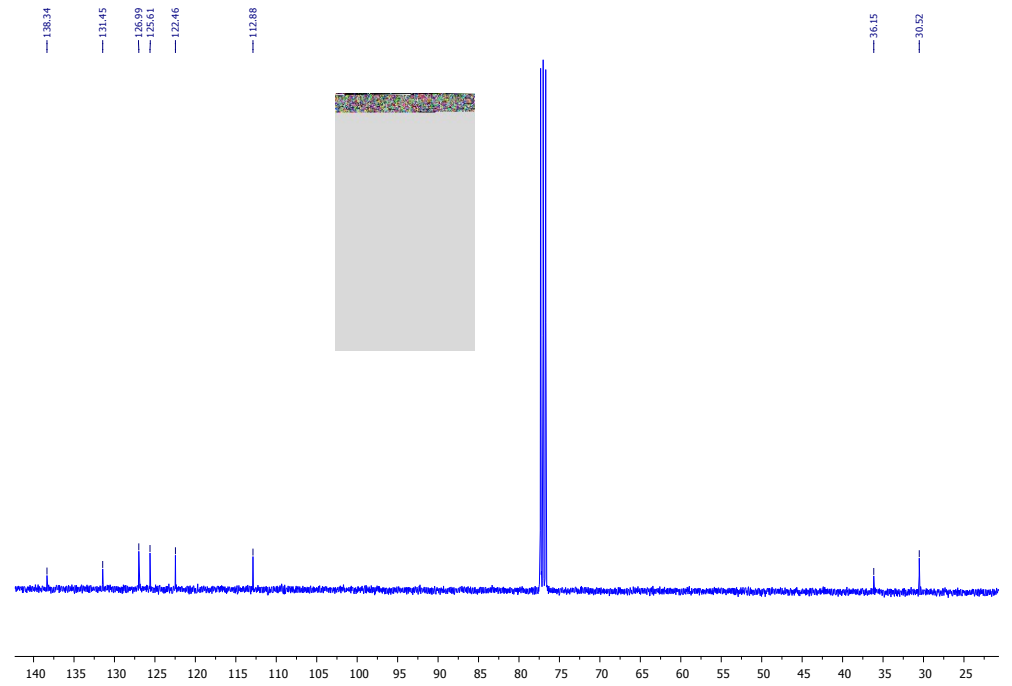
138.34
131.45
126.99
125.61
122.46
112.88
36.15
30.52
140 135 130 125 120 115 110 105 100 95 90 85 80 75 70 65 60 55 50 45 40 35 30 25

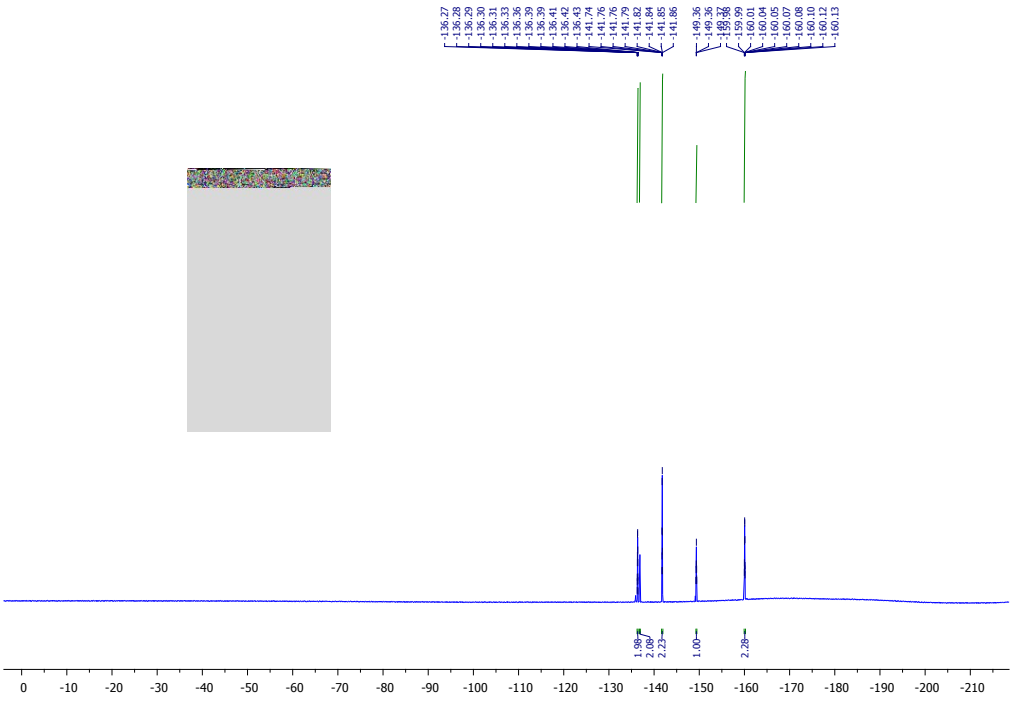
-136.27
-136.28
-136.29
-136.30
-136.31
-136.33
-136.36
-136.39
-136.41
-136.42
-136.43
-141.74
-141.76
-141.78
-141.79
-141.82
-141.84
-141.85
-141.86
-149.36
-149.36
-159.98
-159.99
-160.01
-160.04
-160.05
-160.07
-160.08
-160.10
-160.12
-160.13
1.98
2.08
2.23
1.00
2.28
0 -10 -20 -30 -40 -50 -60 -70 -80 -90 -100 -110 -120 -130 -140 -150 -160 -170 -180 -190 -200 -210

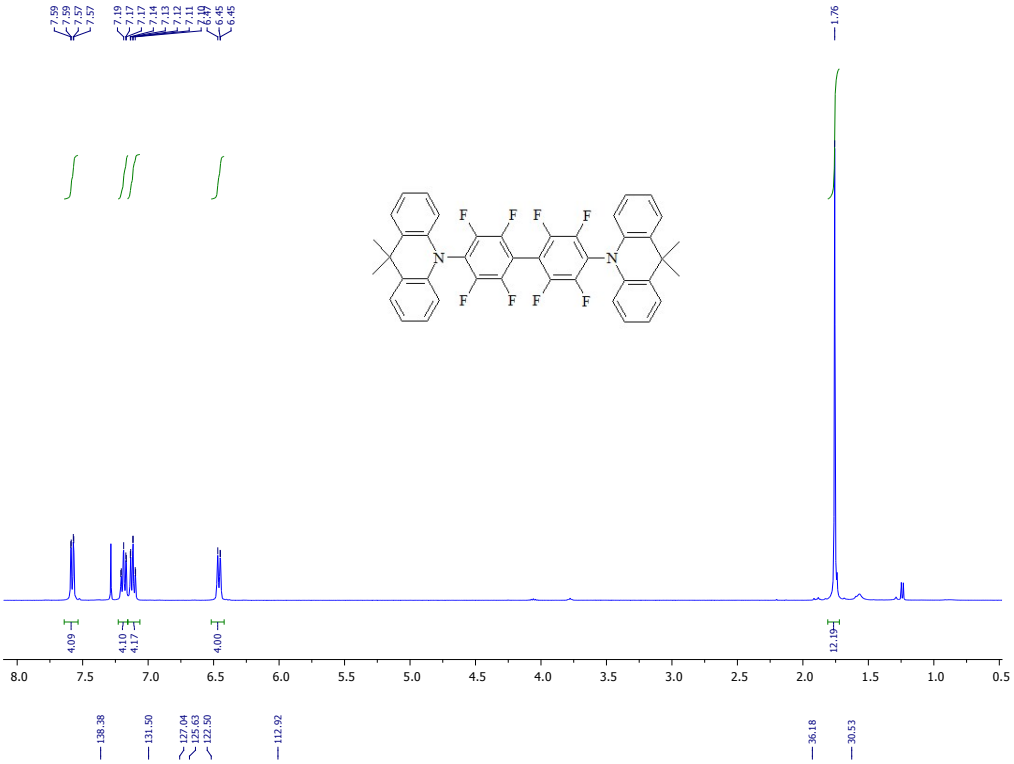
7.59
7.59
7.57
7.57
7.19
7.17
7.17
7.14
7.13
7.12
7.11
6.47
6.45
6.45
1.76
F
F
F
F
F
F
F
F
N
N
4.09
4.10
4.17
4.00
12.19
8.0
7.5
7.0
6.5
6.0
5.5
5.0
4.5
4.0
3.5
3.0
2.5
2.0
1.5
1.0
0.5

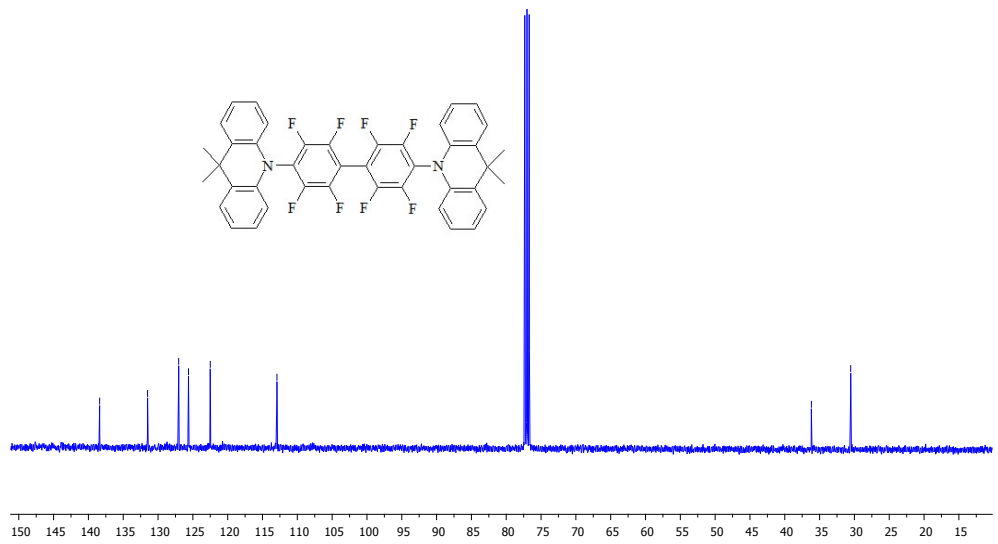
138.38
131.50
127.04
125.63
122.50
112.92
36.18
30.53
F
F
F
F
F
F
F
F
N
N
150
145
140
135
130
125
120
115
110
105
100
95
90
85
80
75
70
65
60
55
50
45
40
35
30
25
20
15

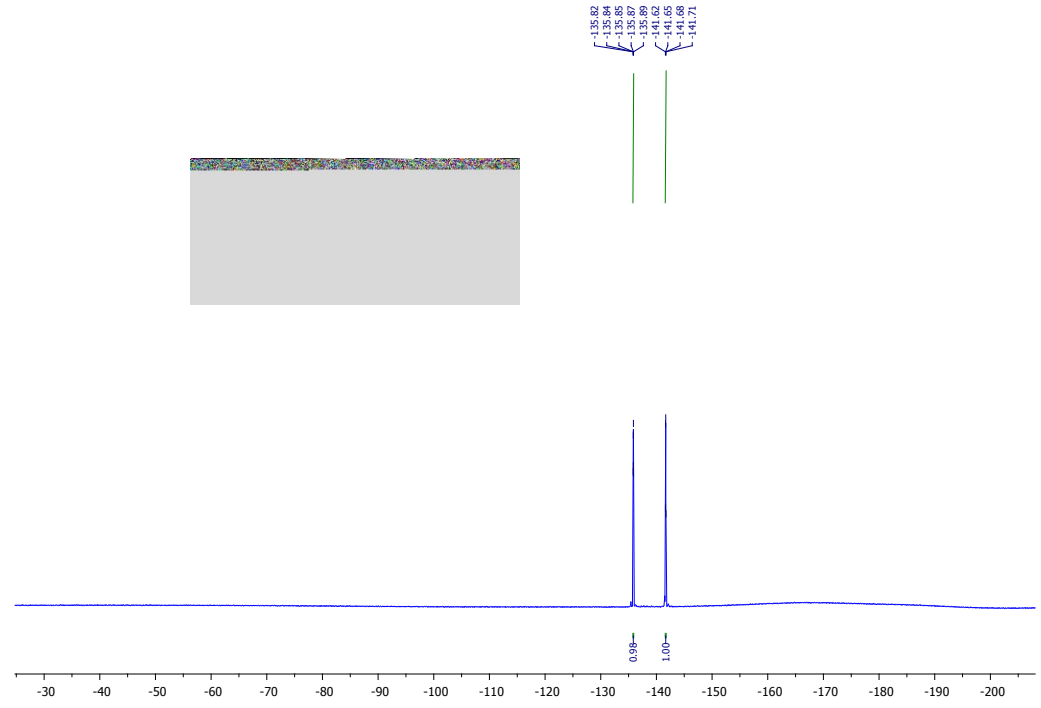
-135.82
-135.84
-135.85
-135.87
-135.89
-141.62
-141.65
-141.68
-141.71
0.98
1.00
-30
-40
-50
-60
-70
-80
-90
-100
-110
-120
-130
-140
-150
-160
-170
-180
-190
-200

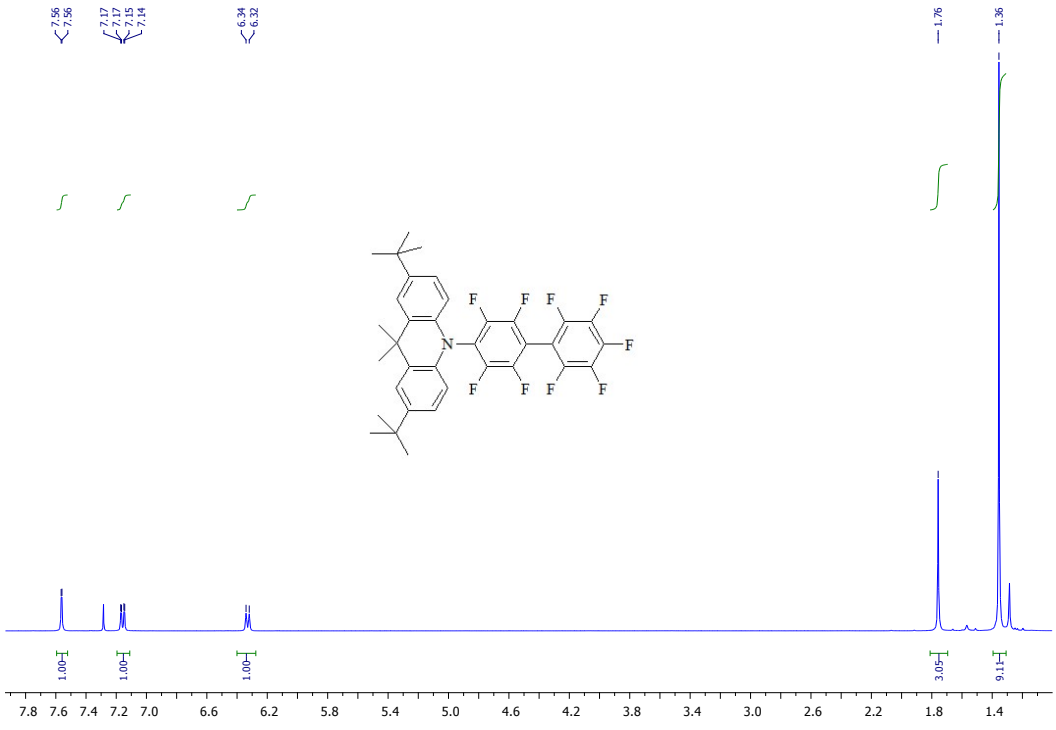
7.56
7.56
7.17
7.17
7.15
7.14
6.34
6.32
1.76
1.36
F
N
1.00
1.00
1.00
3.05
9.11
7.8
7.6
7.4
7.2
7.0
6.6
6.2
5.8
5.4
5.0
4.6
4.2
3.8
3.4
3.0
2.6
2.2
1.8
1.4

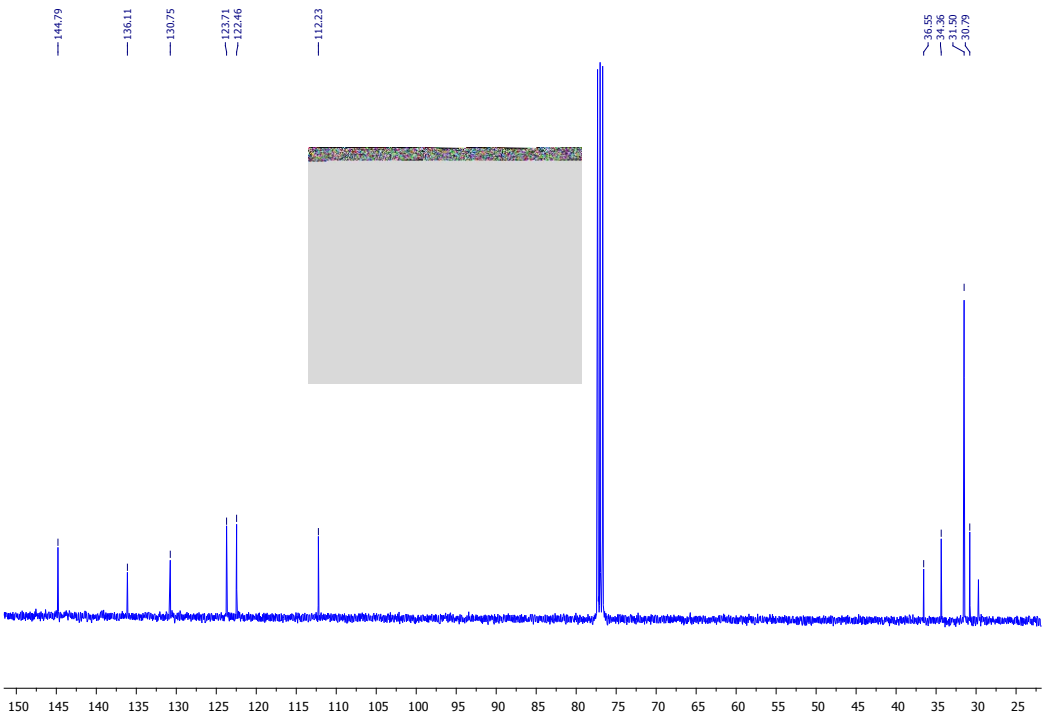
144.79
136.11
130.75
123.71
122.46
112.23
36.55
34.36
31.50
30.79

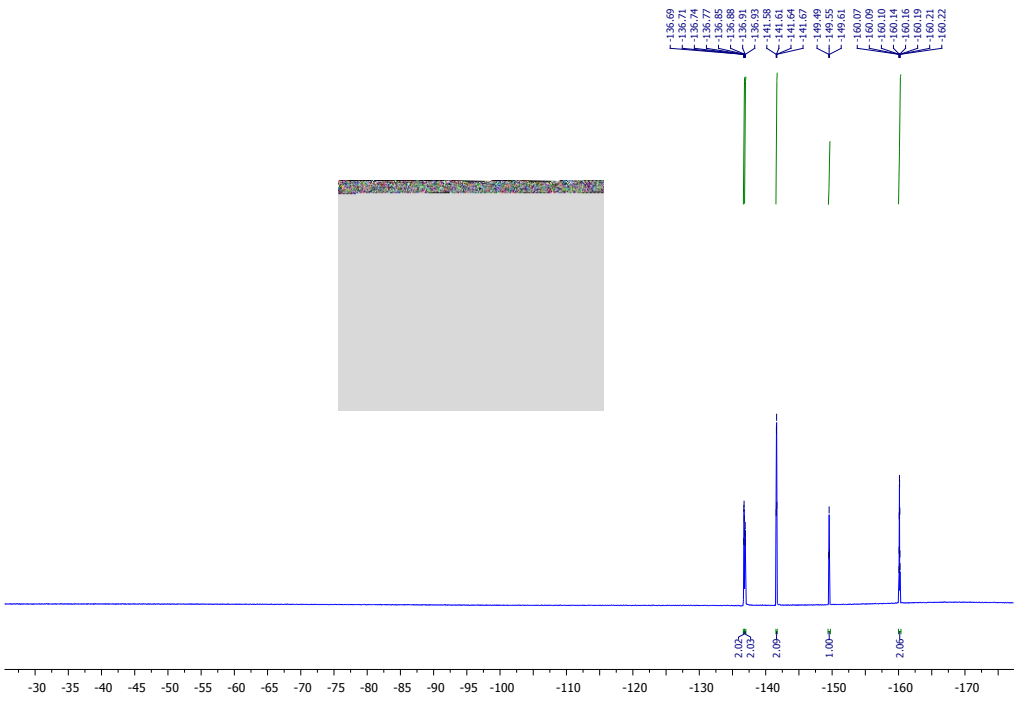
-136.69
-136.71
-136.74
-136.77
-136.85
-136.88
-136.91
-136.93
-141.58
-141.61
-141.64
-141.67
-149.49
-149.55
-149.61
-160.07
-160.09
-160.10
-160.14
-160.16
-160.19
-160.21
-160.22
2.02
2.03
2.09
1.00
2.06

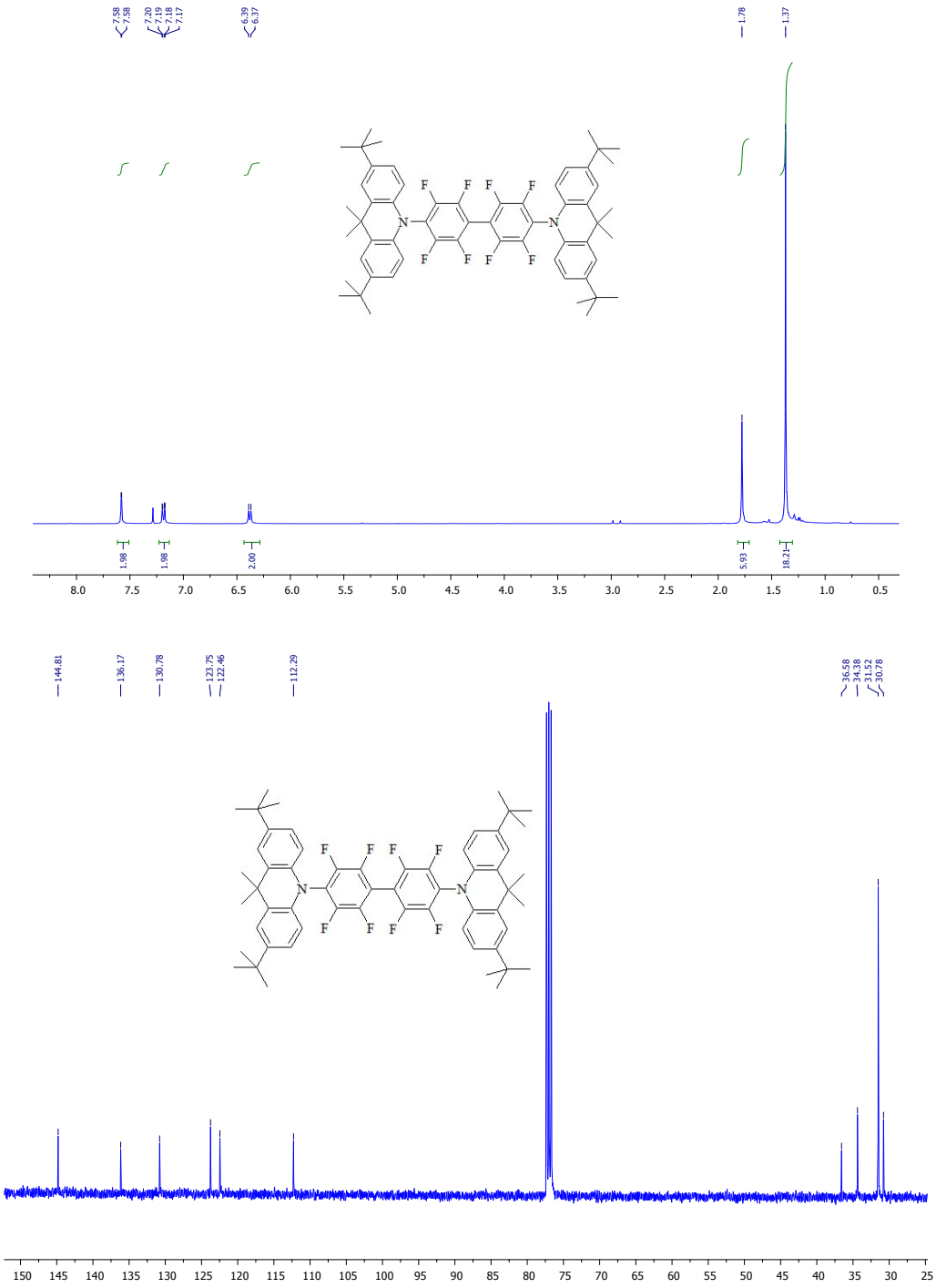
7.58
7.58
7.20
7.19
7.18
7.17
6.39
6.37
1.78
1.37
1.98
1.98
2.00
5.93
18.21
144.81
136.17
130.78
123.75
122.46
112.29
36.58
34.38
31.52
30.78

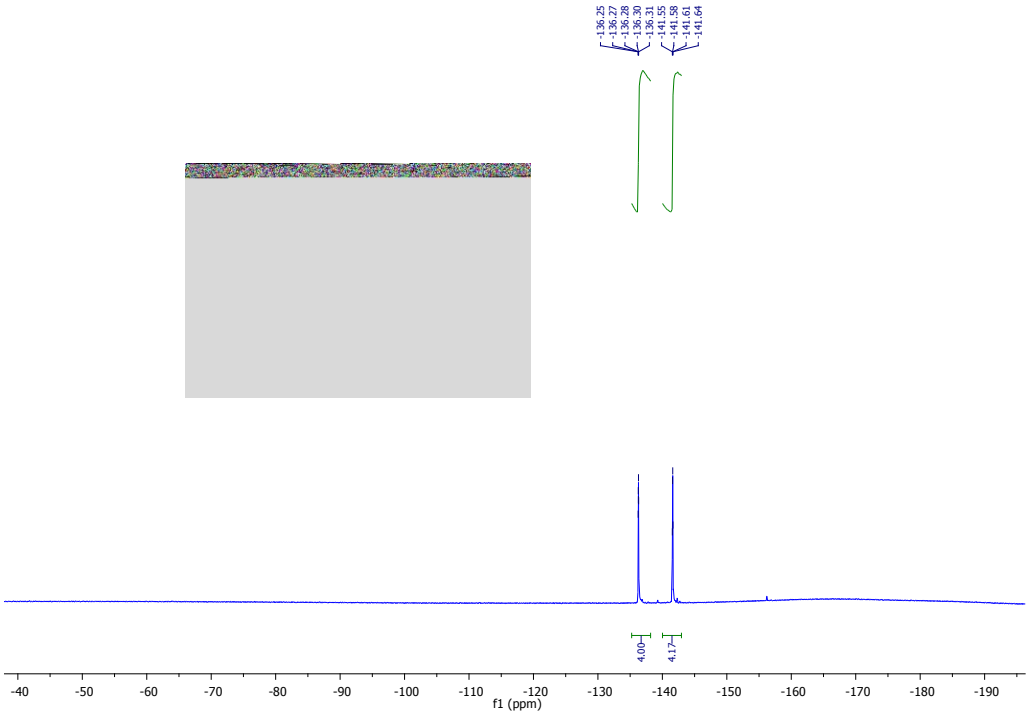

Figure S1. ^{1}H, ^{13}C and ^{19}F NMR spectra of **PFBPs** recorded in $CDCl_3$.

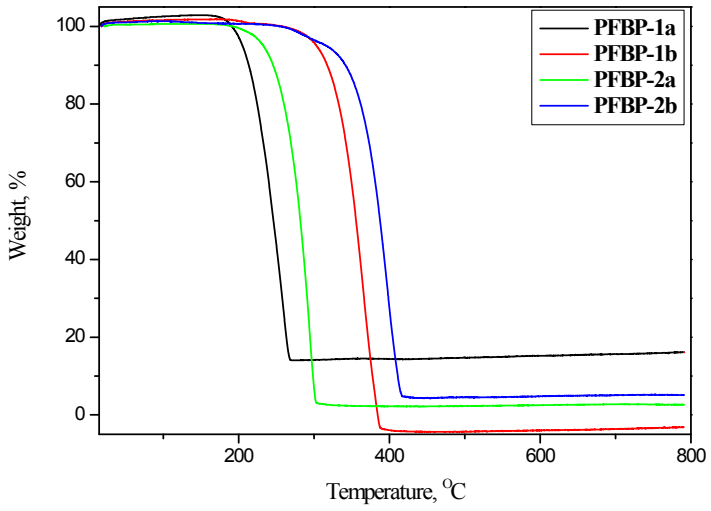

a)

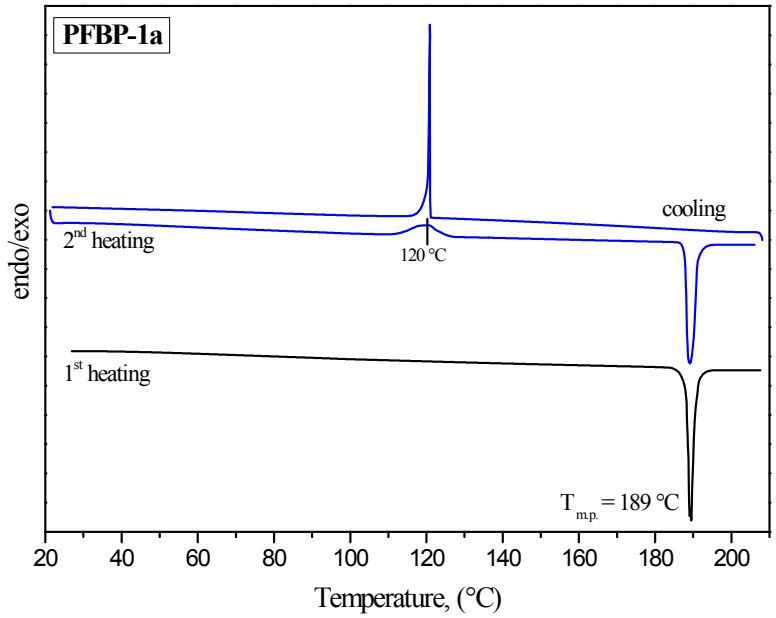
PFBP-1a
endo/exo
cooling
2nd heating
120 °C
1st heating
T m.p. = 189 °C
20 40 60 80 100 120 140 160 180 200
Temperature, (°C)

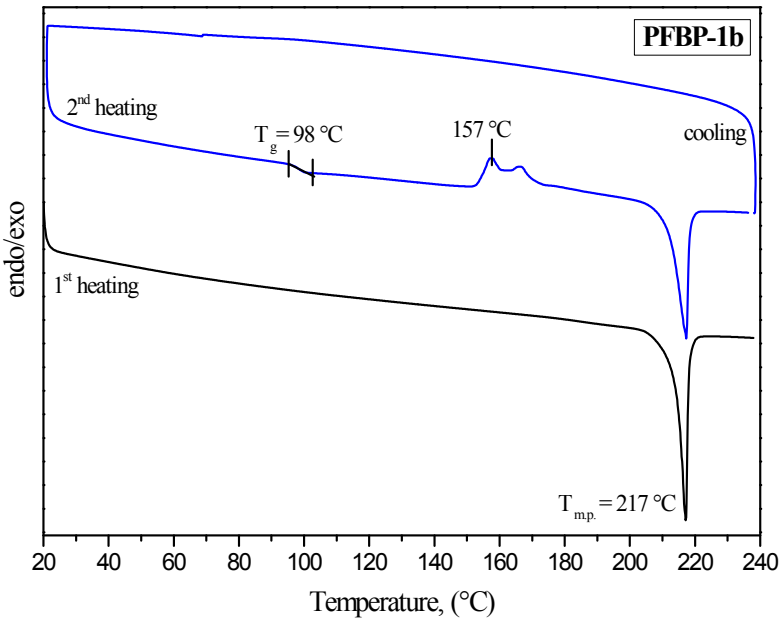
PFBP-1b
endo/exo
2nd heating
T g = 98 °C
157 °C
cooling
1st heating
T m.p. = 217 °C
20 40 60 80 100 120 140 160 180 200 220 240
Temperature, (°C)

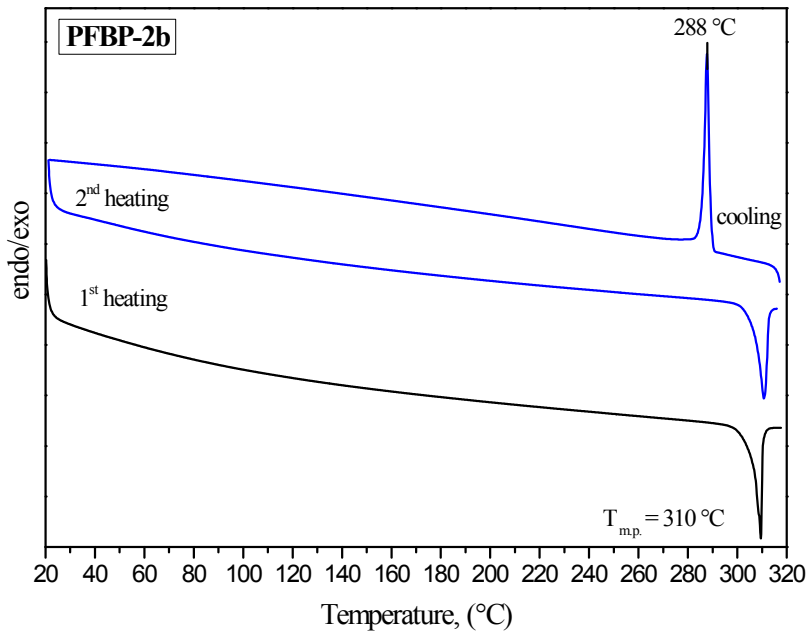
PFBP-2b
288 °C
endo/exo
2nd heating
cooling
1st heating
T m.p. = 310 °C
20 40 60 80 100 120 140 160 180 200 220 240 260 280 300 320
Temperature, (°C)

b)

Figure S2. The thermal characterization of synthesized compounds**:** TGA **(**a) and DSC (b) curves

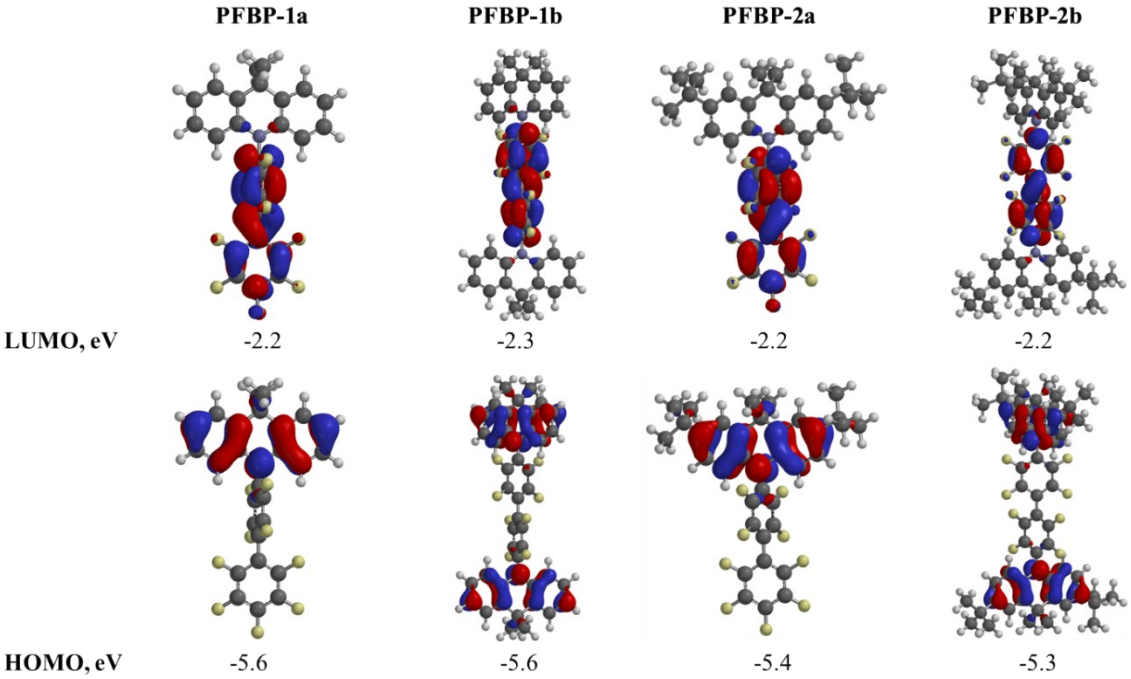

Figure S3. Theoretical calculations for synthesized compounds

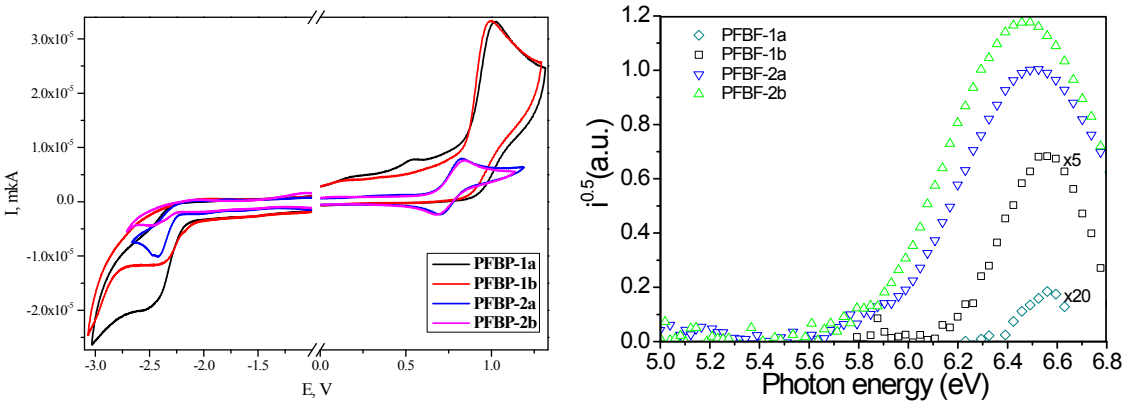

(a) (b)

Figure S4. CV and photoelectrical measurements of synthesized compounds

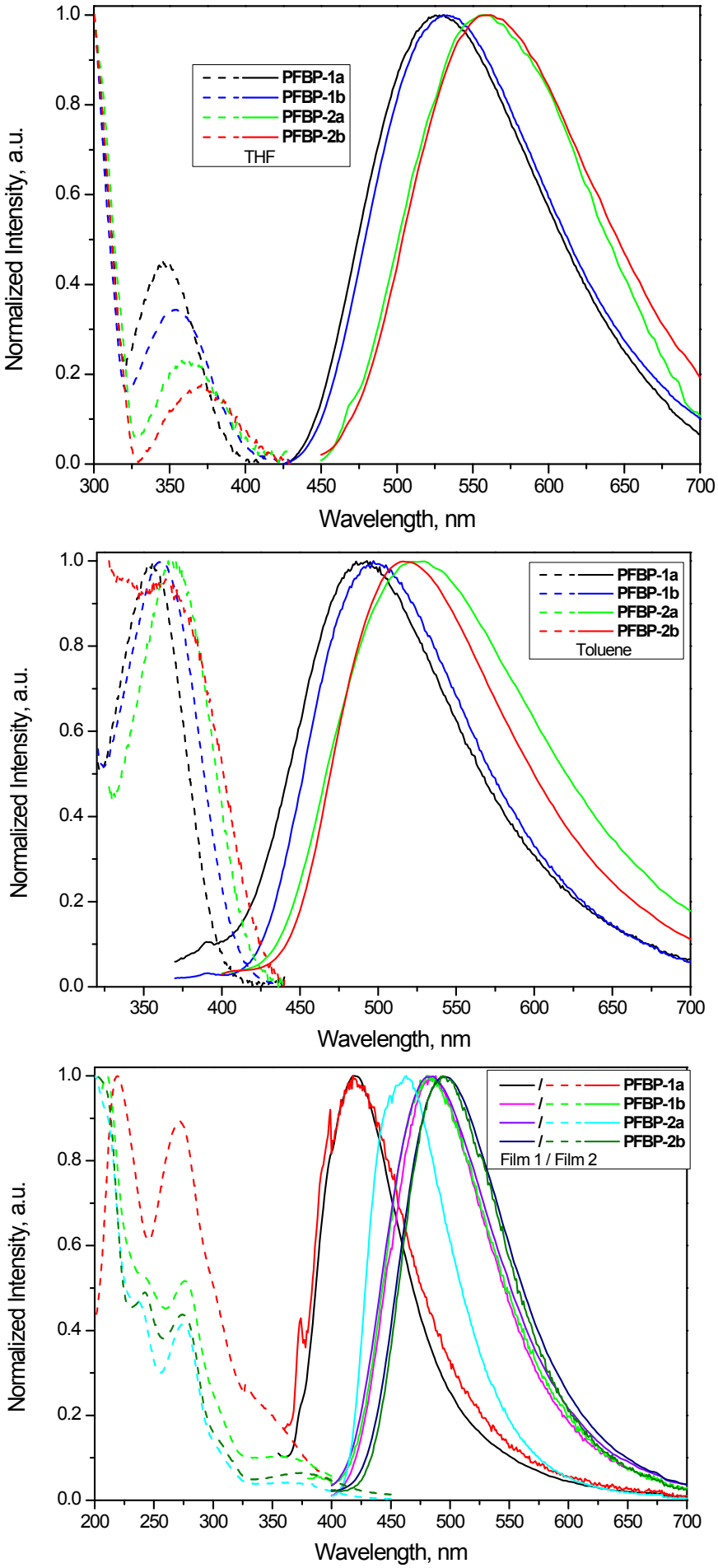

Figure S5. UV and photoluminescence spectra of synthesized compounds in different media

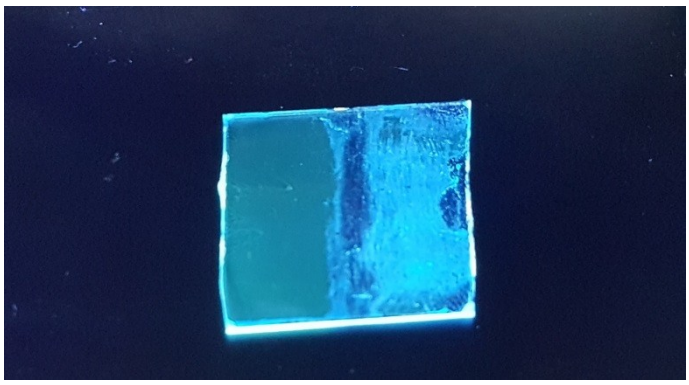

Figure S6. Non-treated (the left side) and mechanically + temperature (<80 °C) treated (the right side) film based on the compound **PFBP-2a** under UV excitation**.** The film was fabricated by the spin-coating.

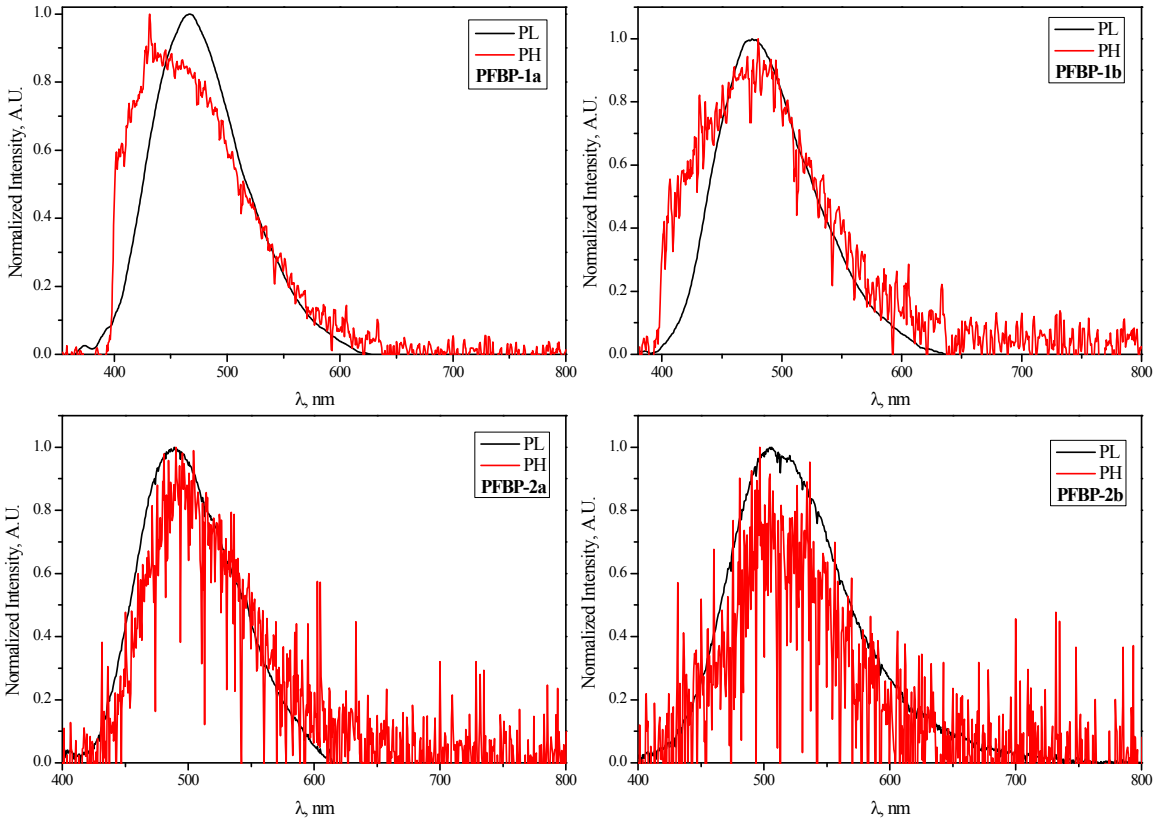

Figure S7. Photoluminescence and phosphorescence spectra and 77K for obtained compounds

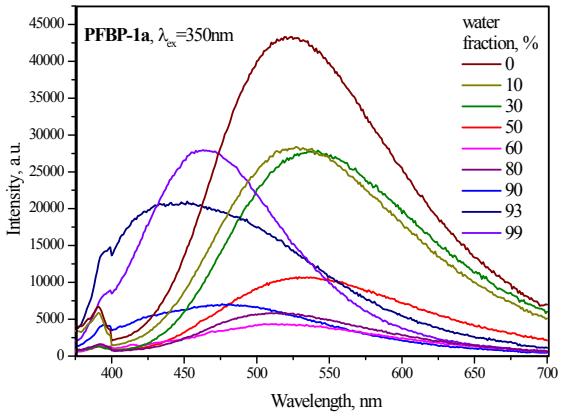
PFBP-1a, λex=350nm
water fraction, %
0
10
30
50
60
80
90
93
99
Intensity, a.u.
Wavelength, nm

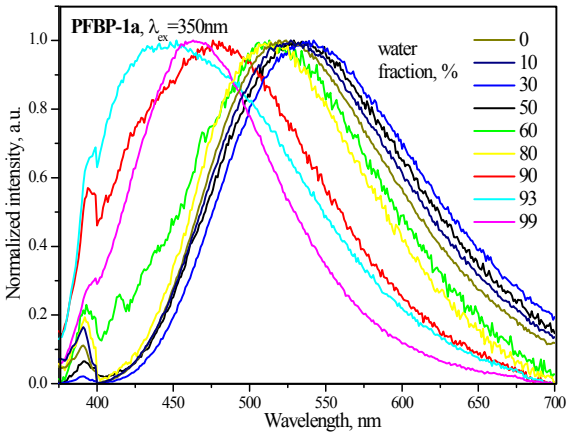
PFBP-1a, λex=350nm
water fraction, %
0
10
30
50
60
80
90
93
99
Normalized intensity, a.u.
Wavelength, nm

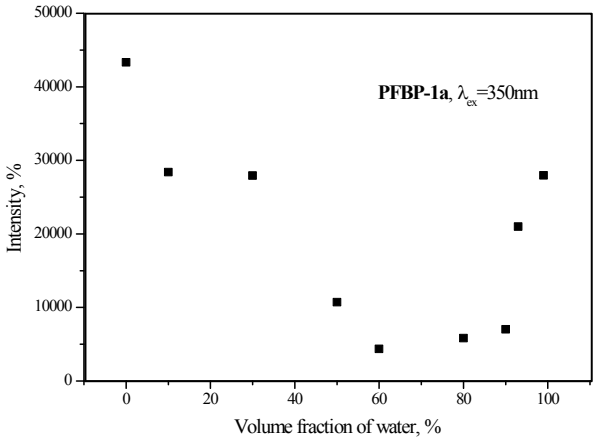
PFBP-1a, λex=350nm
Intensity, %
Volume fraction of water, %

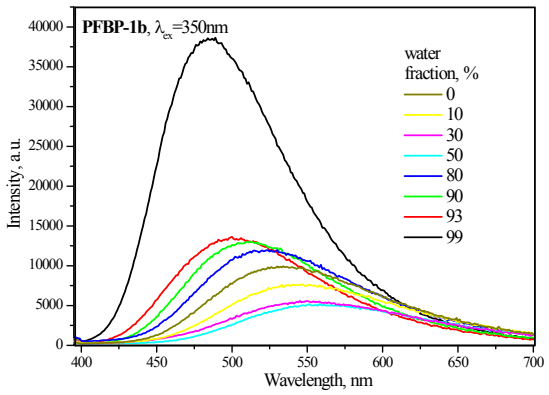
PFBP-1b, λex=350nm
water fraction, %
0
10
30
50
80
90
93
99
Intensity, a.u.
Wavelength, nm

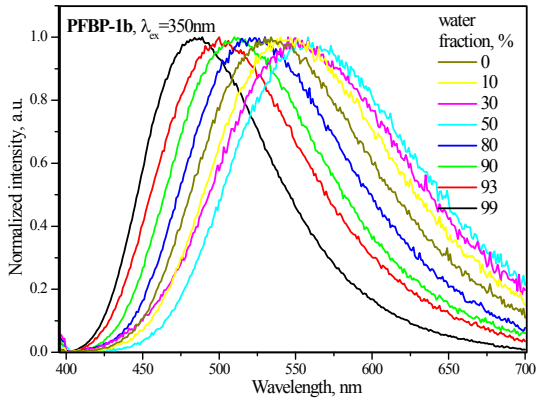
PFBP-1b, λex=350nm
water fraction, %
0
10
30
50
80
90
93
99
Normalized intensity, a.u.
Wavelength, nm

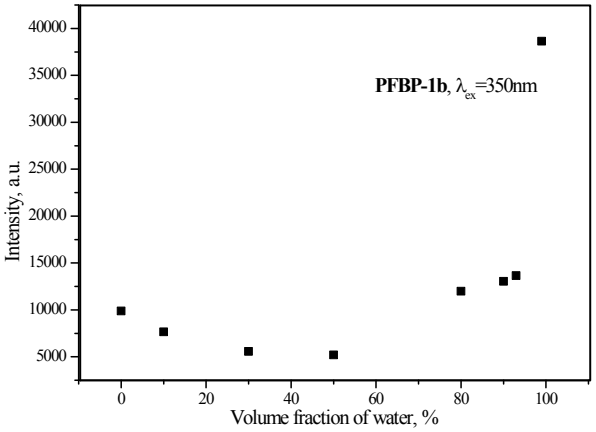
PFBP-1b, λex=350nm
Intensity, a.u.
Volume fraction of water, %

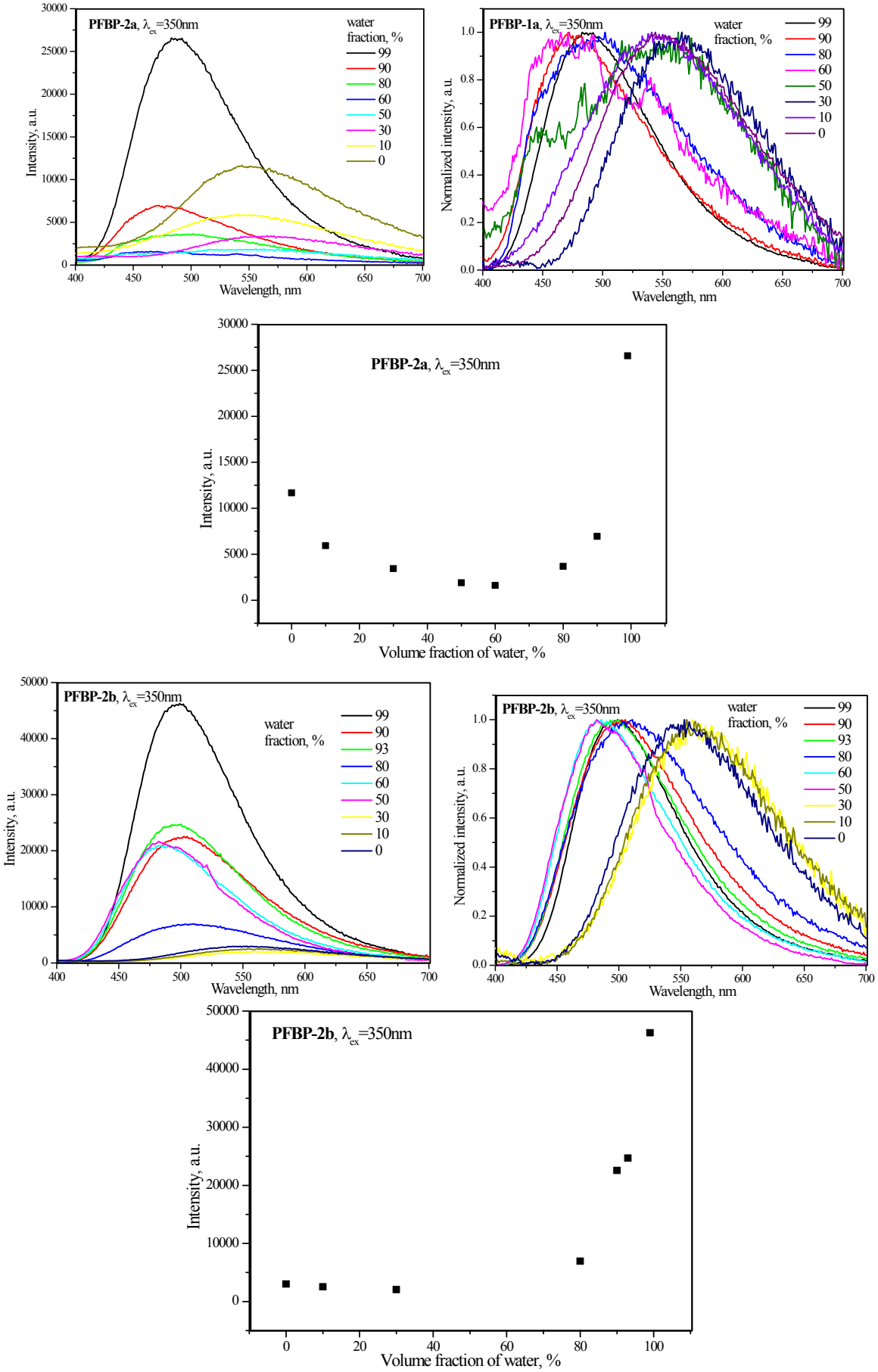

Figure S8. PL spectra of **PFBPs** and PL intensity of the dispersions obtained derivatives in water–THF mixtures with the different water fractions (f_w, vol%)

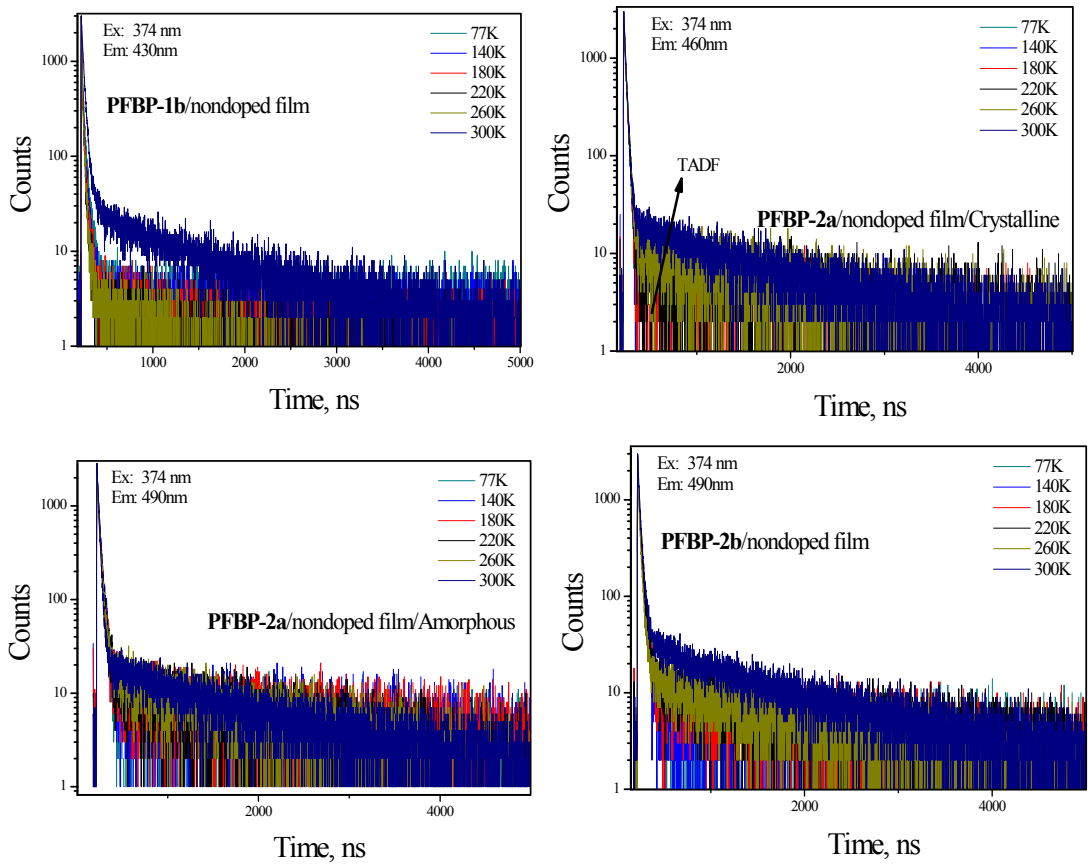

a)

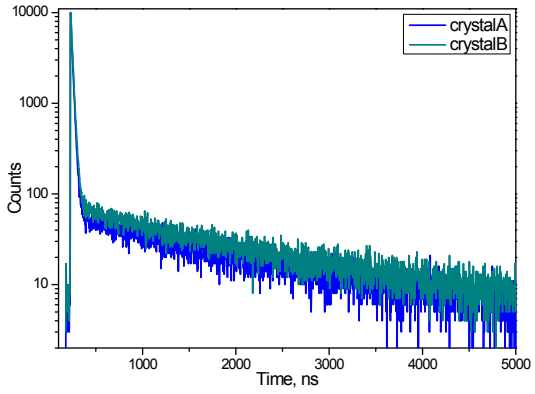

b)

Figure S9. PL decay curves of vacuum deposited layers of **PFBPs** at different temperatures (a) and PL decay curves of crystalline samples of **PFBP-2a_crystaA** and **PFBP-2a_crystaB** (b).

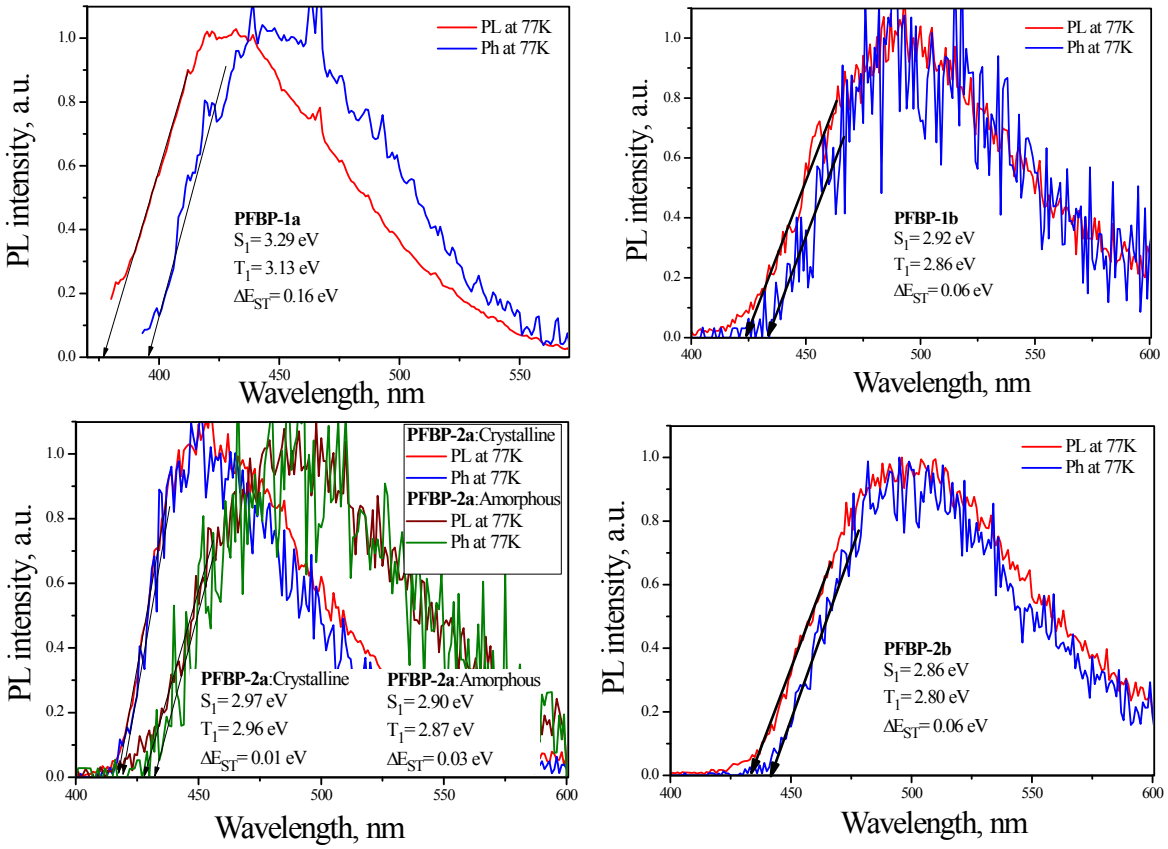

Figure S10. PL and Ph spectra of **PFBPs** films (Ph recorded after 100 μs after excitation)**.**

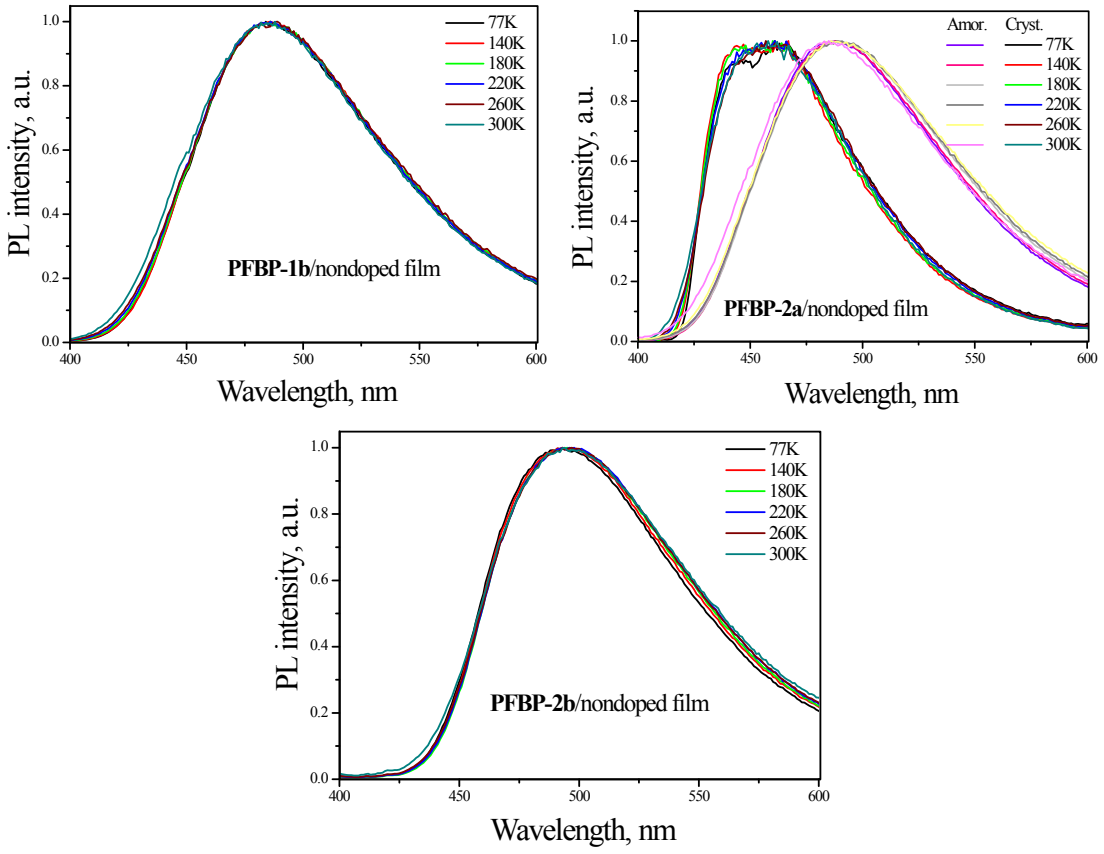

Figure S11. PL of **PFBPs** films recorded at different temperatures under nitrogen atmosphere

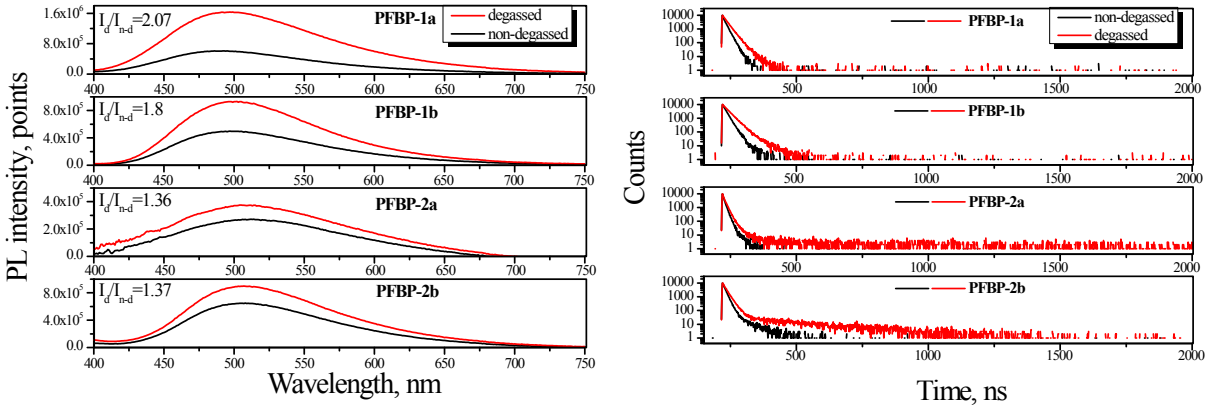

Figure S12. PL spectra (a) and PL decay curves (b) of the solutions of studied derivatives in non-deoxygenated and deoxygenated toluene.

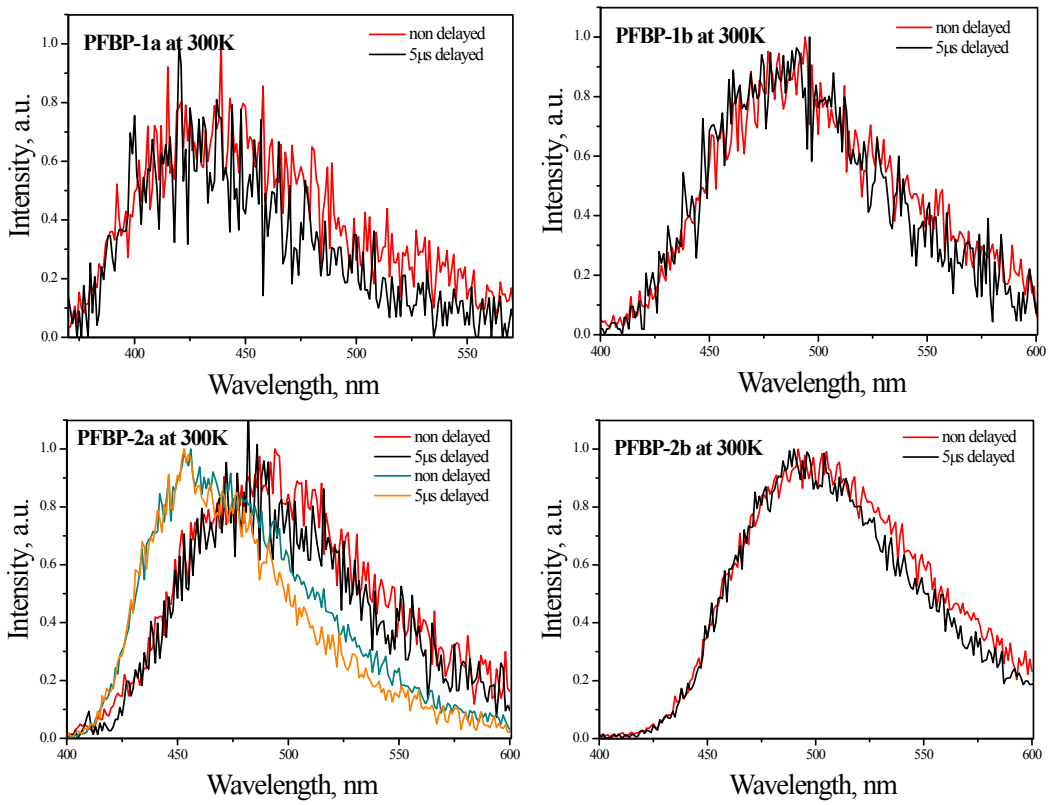

Figure S13. Prompt and delayed PL of **PFBPs** films recorded at 300 K.

Table S1. Hydrogen-bond geometry for compounds **PFBP-1a**, **PFBP-1b**, **PFBP-2a_crystalA** and **PFBP-2a_crystalB** (Å, º)

D–H···A	D–H (Å)	H···A (Å)	D···A (Å)	D–H···A (°)
PFBP-1a				
C3–H3···F19	0.95	2.52	3.371(2)	149
C5–H5···F28	0.95	2.40	3.284(2)	155
PFBP-1b				
C5D–H5D···F25A	0.95	2.48	3.163(6)	129
C13D–H13D···F25C	0.95	2.35	3.273(7)	163
C33B–H33B···F22A	0.95	2.34	3.268(6)	165
PFBP-2a_crystalA				

C39B–H39B···F21	0.96	2.60	3.54(3)	166
PFBP-2a_crystaB				
C32–H32B···F22	0.98	2.53	3.298(3)	135
C40–H40···F19	0.98	2.35	3.265(4)	155

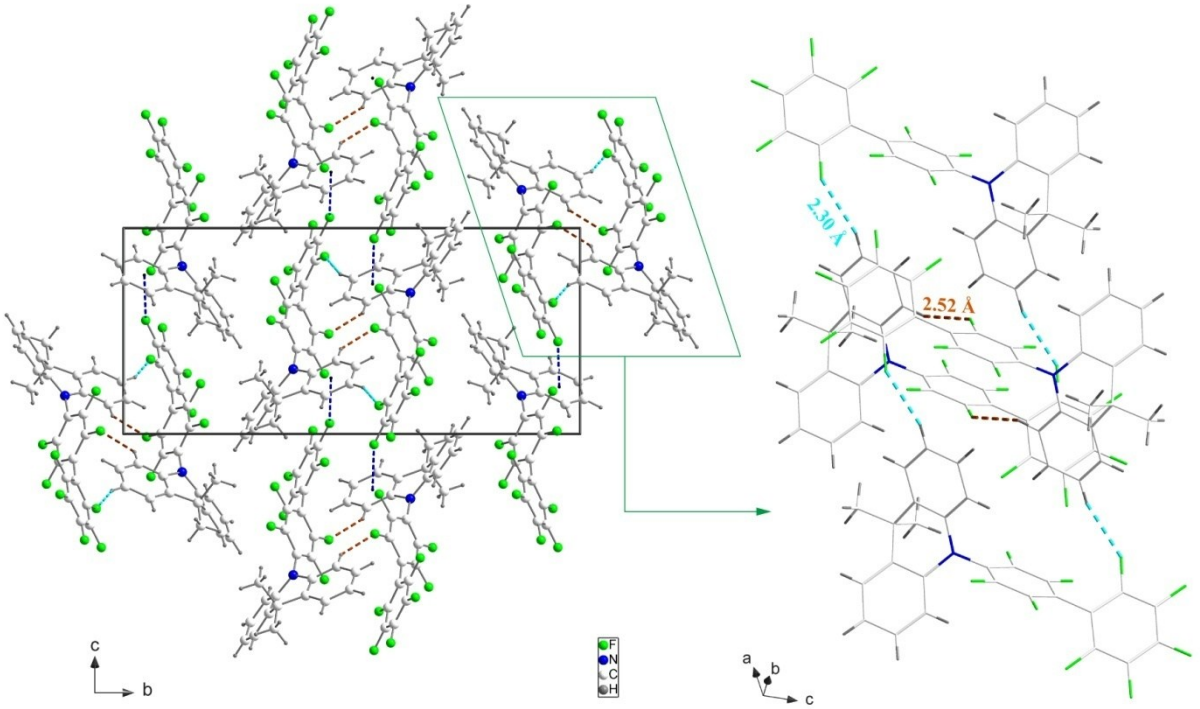

Figure S14. (Left) The molecular arrangement in the **PFBP-1a** compound viewed along [100]. Orange/cyan and blue dashed lines represent C–H···F hydrogen bonds and C–F···π interactions, respectively. (Right) A cluster of four molecules, forming by two unique C–H···F interactions.

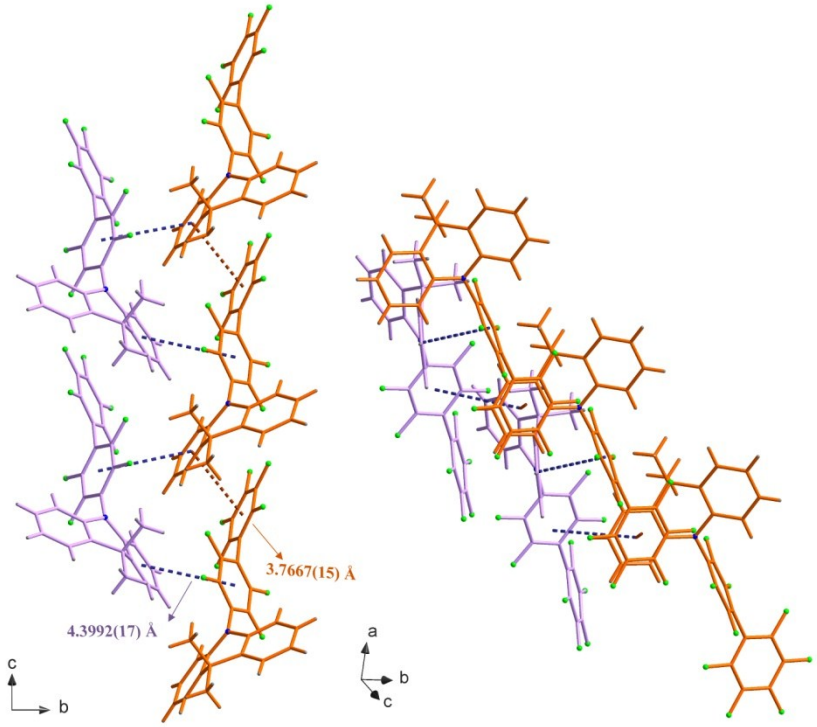

Figure S15. The π-π interactions between neighbouring DMAC-PFBP molecules in the **PFBP-1a** compound.

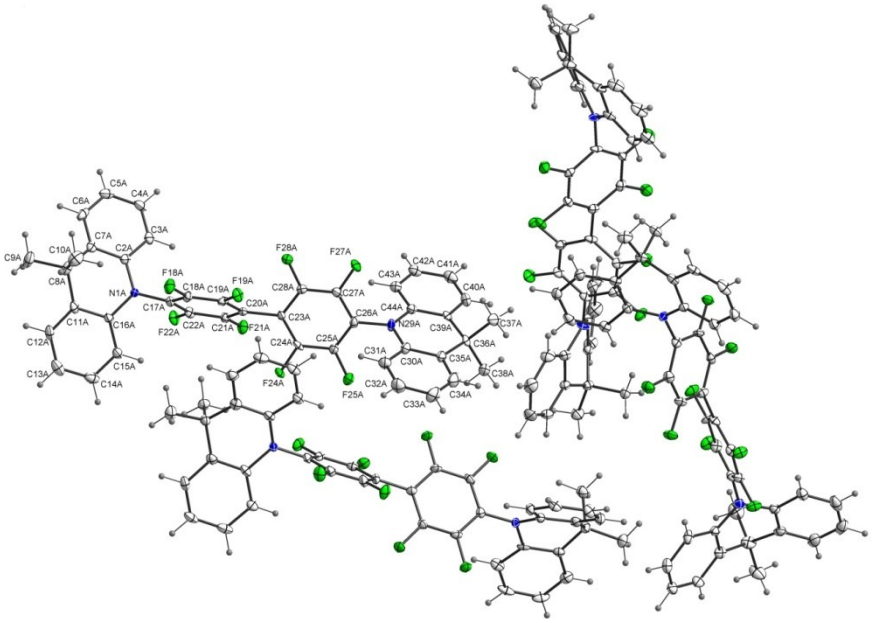

Figure S16. The asymmetric unit of **PFBP-1b** compound, showing the atom-numbering scheme for molecule A. Displacement ellipsoids are drawn at the 50 % probability level.

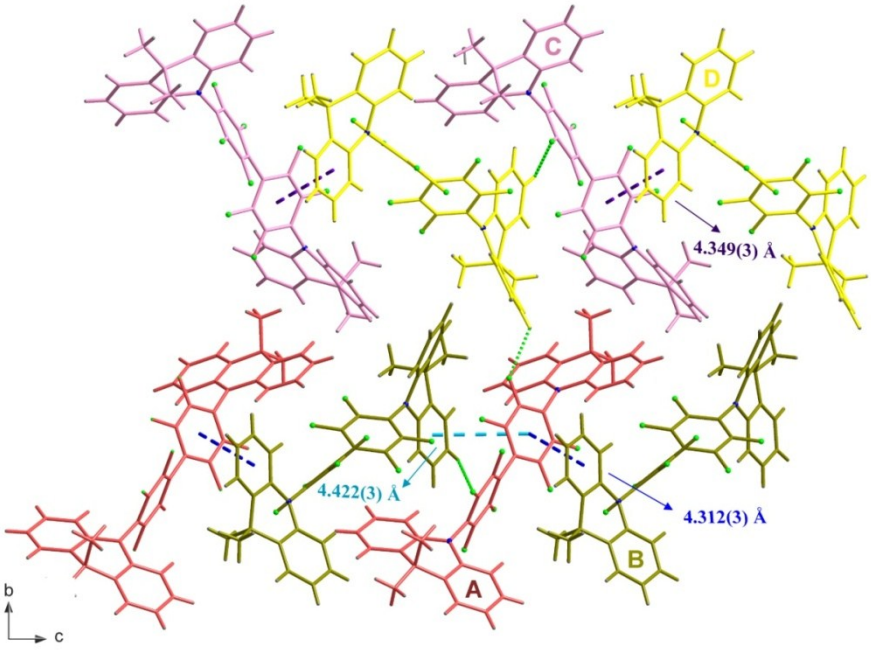

Figure S17. The part of crystal packing of **PFBP-1b** viewed along [100]. The colorful thick bonds represent four independent DMAC-PFBP molecules. Cyan, violet and blue dashed lines represent π-π interactions.

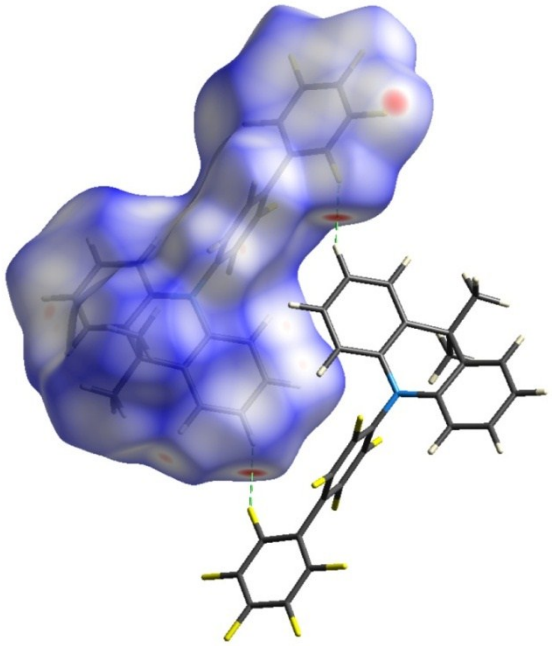

Figure S18. Hirshfeld surface of two neighbouring molecules in compound **PFBP-1a**.

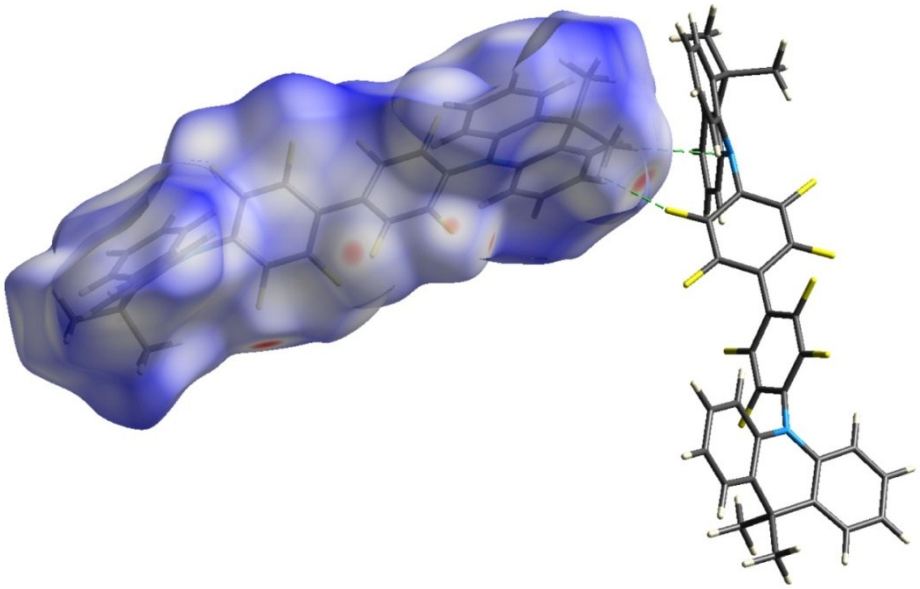

Figure S19. Hirshfeld surface of two neighbouring molecules in compound **PFBP-1b**.

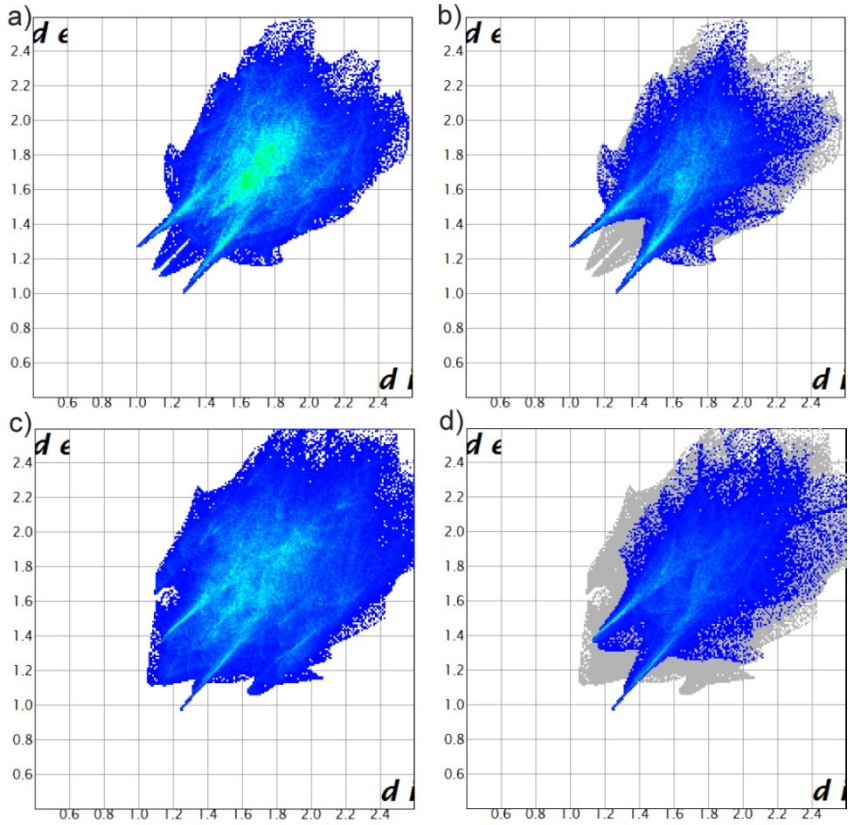

Figure S20. a) Two-dimensional fingerprint plots of DMAC-PFBP molecules and b) fingerprint plots of contribution of H…F contacts in compound **PFBP-1a**. c) Two-dimensional fingerprint plots of DMAC-PFBP molecules and d) fingerprint plots of contribution of H…F contacts in compound **PFBP-1b**.

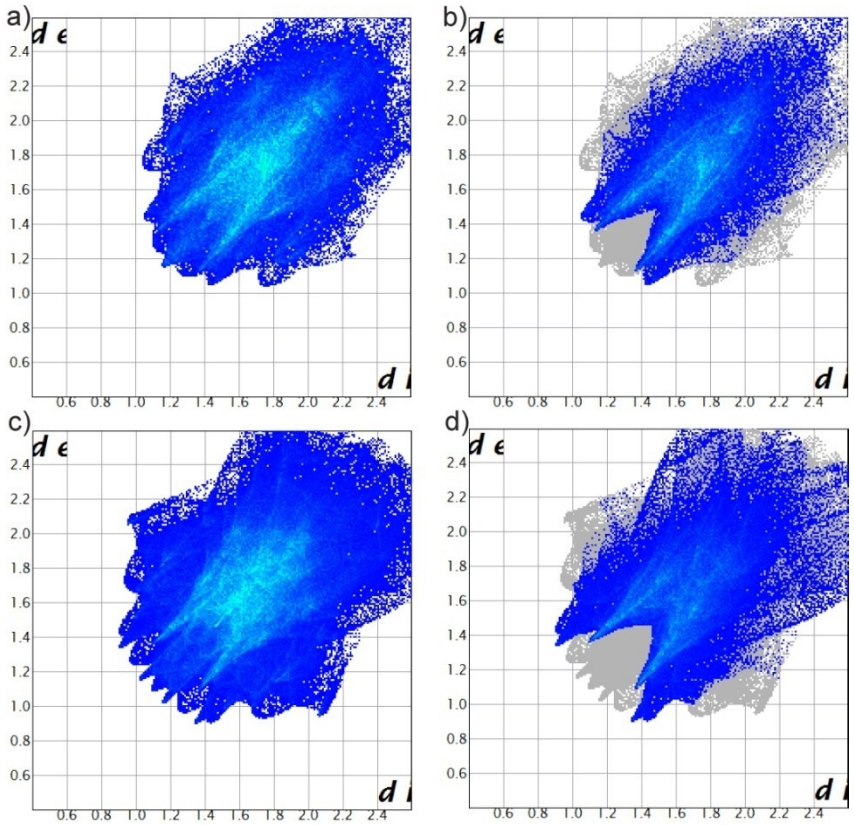

Figure S21. a) Two-dimensional fingerprint plots of DMAC-PFBP molecules and b) fingerprint plots of contribution of H…F contacts in compound **PFBP-2a_crystalA** and c) Two-dimensional fingerprint plots of DMAC-PFBP molecules and d) fingerprint plots of contribution of H…F contacts in compound **PFBP-2a_crystaB**.

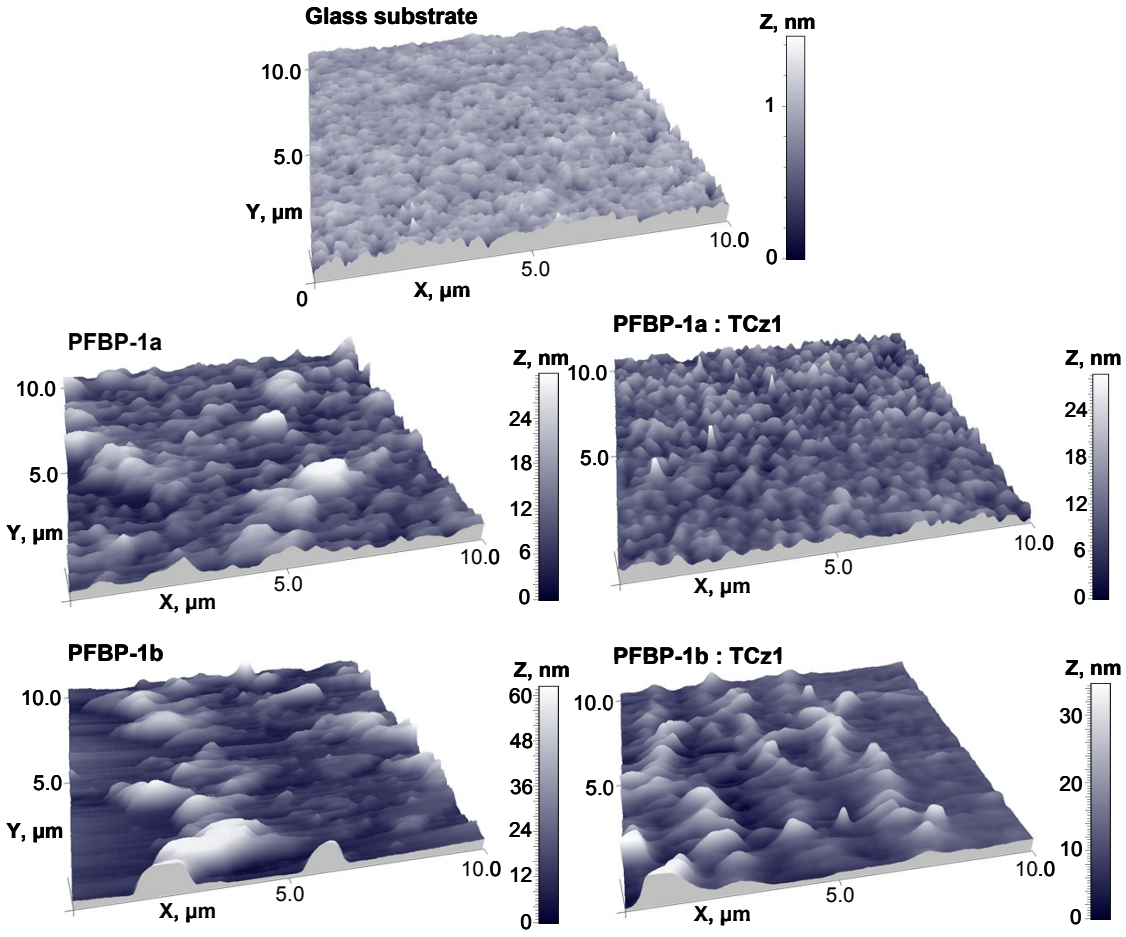

Sample	Rougness parameters			
	R_q	R_{sk}	R_{ku}	Z_{mean}
Glass substrate	0.13	-1.33	6.29	0.87
PFBP-1a	4.74	1.11	4.60	11.09
PFBP-1a:TCz1	3.11	0.50	3.62	10.37
PFBP-1b	10.66	1.56	5.48	19.92
PFBP-1b:TCz1	4.92	1.25	5.40	12.52

Figure S22. (top) AFM 3D topographical images of vacuum deposited thin films as well as glass substrate. (bottom) summary of roughness parameters.

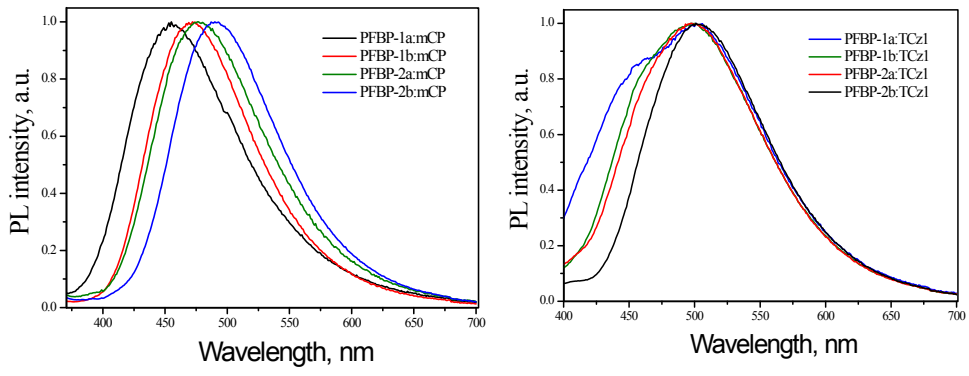

(a)

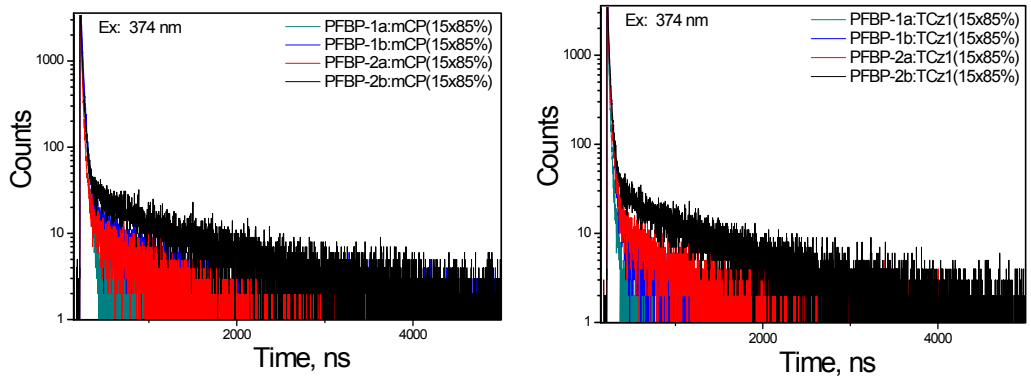

(b)

Figure S23. PL spectra (a) and PL decay curves (b) of doped films.

Table S2. PL characteristics of doped films of **PFBPs**

N/N	**PFBP-1a**	**PFBP-1b**	**PFBP-2a**	**PFBP-2b**
λ_{max}(mCP), nm	455	472	477	490
Φ (mCP)	0.15	0.45	0.15	0.22
λ_{max}(TCz1), nm	501	497	498	501
Φ (TCz1)	0.37	0.47	0.47	0.73

Owing to donor-acceptor structure of the compounds, bipolar charge carrier transport was expected. To study the impact of donor substituents on charge-transporting properties of the vacuum-deposited films, time-of-flight (ToF) measurements we performed generating holes or electrons on the ITO/film interfaces by light excitation through the ITO electrode using a pulsed laser (λ = 355 nm) and different polarity of applied voltages (plus on ITO for holes, minus for electrons). Thus, the photogenerated either holes or electrons were transported through the layer from ITO electrode to the opposite Al electrode under different external electric fields.

Very dispersive charge transport was observed by TOF experiment. It was very difficult to take the transit times (t_{tr}) for the studied samples at different applied electric fields (voltages (U)) for holes and electrons from the corresponding photocurrent transients in log-log scales for the all tested samples. This resulted in considerable errors. (Figure S24). We tried to define the t_{tr} for **PFBP-2b** as it is shown in Figure S4. Hole mobility (μ_h) of ca. 1.0×10^{-4} $cm^2V^{-1}s^{-1}$ at electric field of 6×10^5 Vcm^{-1} for **PFBP-2b** was estimated using equation $\mu_h(\mu_e)=d^2/(U\times t^{tr})$ (Figure S25).

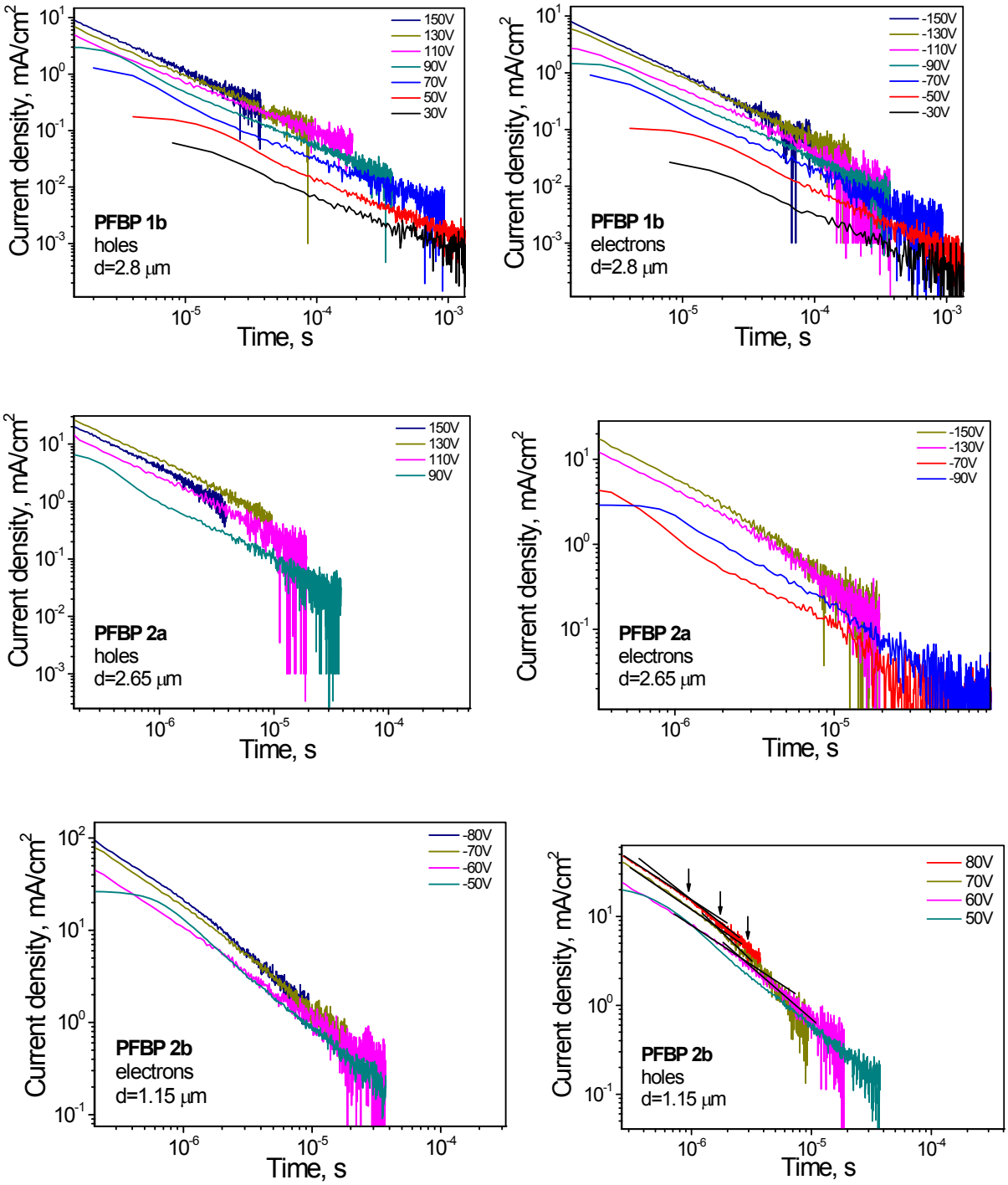

Figure S24. Electron and hole time-of-flight current transients for the studied samples **PFBP-1b, PFBP-2a,** and **PFBP-2b**.

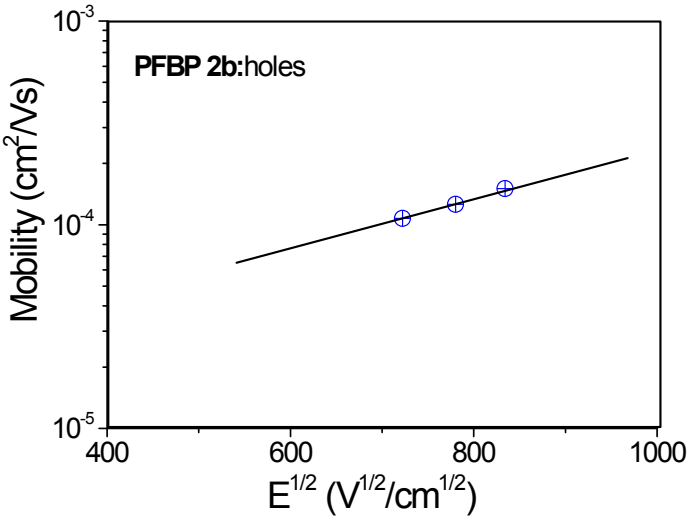

Figure S25. Hole mobility versus electric fields for the **PFBP-2b**.

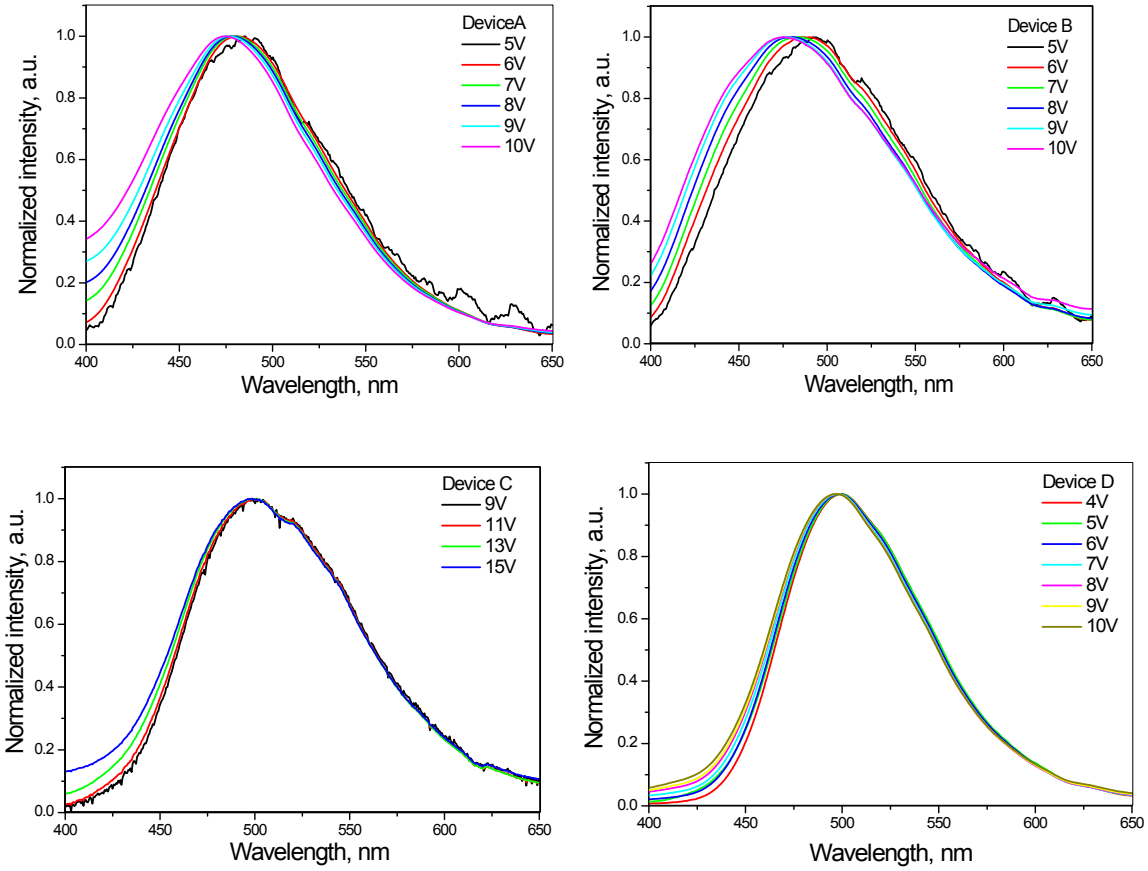

Figure S26. EL spectra of the studied devices at different voltages.

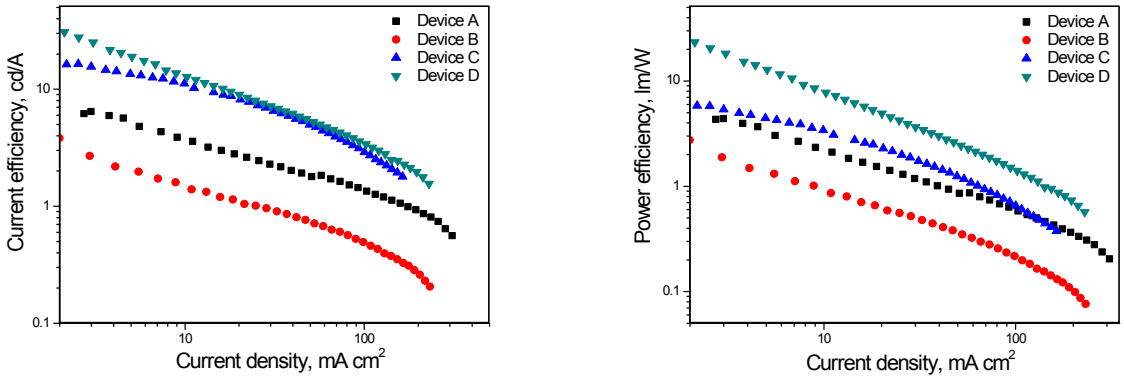

Figure S27. Current and power efficiencies of the studied devices.

Supporting information

1. Experimental details

1.1 Instrumentation

(before Powder X-ray diffraction)

The intensity data for compounds **PFBP-1a**, **PFBP-1b** and **PFBP-2b_crystalB** were collected at 100 K on an Oxford Diffraction Xcalibur diffractometer equipped with graphite-monochromated Mo Ka radiation (λ = 0.71073 Å). The instrument was equipped with an Oxford Cryosystems 800 series cryocooler. Data collection and reduction were made using CrysAlisCCD and CrysAlis RED programs (Rigaku, 2015). The crystallographic measurement for compound **PFBP-2b_crystalA** was performed at 295 K on a XtaLAB Mini (ROW) diffractometer. A numerical absorption correction based on the shape of the crystals was performed. The crystal structures were solved by direct methods and all non-hydrogen atoms were refined anisotropically with full-matrix least-squares techniques on F^2 by SHELXL with the following graphical user interfaces of OLEX^2 (Sheldrick, 2015; Dolomanov *et al.*, 2009). For all structures H-atom parameters were constrained. In compound **PFBP-2a_crystalA** one of two *tert*-butyl groups is disordered over two positions with site occupancies of 0.645(15) and 0.355(15). In order to avoid the distortion of the disordered *tert*-butyl group, SHELXL (SADI, DELU and SIMU) instructions were used. In compound **PFBP-2a_crystalB** both *tert*-butyl functional groups are disordered over two sets of sites, with occupancy ratio of 0.538(5):0.462(5) and 0.937(3):0.063(3). The second disordered *tert*-butyl group was refined with distance and angles restraints, and the minor component atoms C33-C35 were refined isotropically.

Details on the single crystal X-ray data collection, reduction and structure parameters for all compounds are given in Tables S2-S5.

(To the end of the Supporting information)

Tables S2. Experimental details for compound **PFBP-1a**

Crystal data	
Chemical formula	$C_{27}H_{14}F_9N$
M_r	523.39
Crystal system, space group	Monoclinic, $P2_1/c$
Temperature (K)	100
a, b, c (Å)	8.834 (3), 23.095 (6), 11.074 (4)
β (°)	109.65 (3)
V (Å^3)	2127.8 (12)
Z	4
Radiation type	Mo $K\alpha$
μ (mm^{-1})	0.15
Crystal size (mm)	0.26 × 0.24 × 0.06
Data collection	
Diffractometer	Xcalibur, Atlas
Absorption correction	Multi-scan *CrysAlis PRO* 1.171.38.46 (Rigaku Oxford Diffraction, 2015) Empirical absorption correction using spherical harmonics, implemented in SCALE3 ABSPACK scaling algorithm.
T_{min}, T_{max}	0.991, 1.000
No. of measured, independent and observed [$I > 2\sigma(I)$] reflections	37368, 5527, 4407
R_{int}	0.027
$(\sin\theta/\lambda)_{max}$ (Å^{-1})	0.694
Refinement	
$R[F^2 > 2\sigma(F^2)]$, $wR(F^2)$, S	0.037, 0.093, 1.02
No. of reflections	5527
No. of parameters	336
H-atom treatment	H-atom parameters constrained
$\Delta\rho_{max}$, $\Delta\rho_{min}$ (e Å^{-3})	0.34, −0.25

Computer programs: *CrysAlis PRO* 1.171.38.46 (Rigaku OD, 2015), ShelXT (Sheldrick, 2015), *SHELXL* (Sheldrick, 2015), Olex2 (Dolomanov *et al.*, 2009).

Tables S3. Experimental details for compound **PFBP-1b**

Crystal data	
Chemical formula	$C_{42}H_{28}F_8N_2$
M_r	712.66
Crystal system, space group	Monoclinic, $P2_1$
Temperature (K)	100
a, b, c (Å)	8.791 (3), 50.622 (9), 15.001 (4)
β (°)	96.16 (3)
V (Å^3)	6637 (3)
Z	8
Radiation type	Mo $K\alpha$
μ (mm^{-1})	0.12
Crystal size (mm)	0.53 × 0.29 × 0.05
Data collection	
Diffractometer	Xcalibur, Atlas
Absorption correction	Multi-scan *CrysAlis PRO* 1.171.38.46 (Rigaku Oxford Diffraction, 2015) Empirical absorption correction using spherical harmonics, implemented in SCALE3 ABSPACK scaling algorithm.
T_{min}, T_{max}	0.818, 1.000
No. of measured, independent and observed [$I > 2\sigma(I)$] reflections	70499, 31163, 23810
R_{int}	0.056
$(\sin \theta/\lambda)_{max}$ (Å^{-1})	0.694
Refinement	
$R[F^2 > 2\sigma(F^2)]$, $wR(F^2)$, S	0.063, 0.150, 1.06
No. of reflections	31163
No. of parameters	1889
No. of restraints	1
H-atom treatment	H-atom parameters constrained
$\Delta\rho_{max}$, $\Delta\rho_{min}$ (e Å^{-3})	0.34, −0.34
Absolute structure	Flack x determined using 8244 quotients [(I+)-(I-)]/[(I+)+(I-)]

	(Parsons, Flack and Wagner, Acta Cryst. B69 (2013) 249-259).
Absolute structure parameter	0.3 (3)

Computer programs: *CrysAlis PRO* 1.171.38.46 (Rigaku OD, 2015), ShelXT (Sheldrick, 2015), *SHELXL* (Sheldrick, 2015), Olex2 (Dolomanov *et al.*, 2009).

Tables S4. Experimental details for compound **PFBP-2b_crystalA**

Crystal data	
Chemical formula	$C_{35}H_{30}F_9N$
M_r	635.60
Crystal system, space group	Monoclinic, $P2_1/c$
Temperature (K)	293
a, b, c (Å)	10.870 (4), 24.126 (6), 12.550 (4)
β (°)	105.57 (3)
V (Å^3)	3170.5 (18)
Z	4
Radiation type	Mo $K\alpha$
μ (mm^{-1})	0.11
Crystal size (mm)	0.38 × 0.35 × 0.05
Data collection	
Diffractometer	XtaLAB Mini (ROW)
Absorption correction	Analytical *CrysAlis PRO* 1.171.39.46 (Rigaku Oxford Diffraction, 2018) Analytical numeric absorption correction using a multifaceted crystal model based on expressions derived by R.C. Clark & J.S. Reid. (Clark, R. C. & Reid, J. S. (1995). Acta Cryst. A51, 887-897) Empirical absorption correction using spherical harmonics, implemented in SCALE3 ABSPACK scaling algorithm.
T_{min}, T_{max}	0.968, 0.994
No. of measured, independent and observed [$I > 2\sigma(I)$] reflections	13429, 6480, 2086
R_{int}	0.133
$(\sin \theta/\lambda)_{max}$ (Å^{-1})	0.625
Refinement	

$R[F^2 > 2\sigma(F^2)]$, $wR(F^2)$, S	0.096, 0.336, 0.91
No. of reflections	6480
No. of parameters	445
No. of restraints	106
H-atom treatment	H-atom parameters constrained
$\Delta\rho_{max}$, $\Delta\rho_{min}$ (e Å^{-3})	0.31, −0.33

Computer programs: *CrysAlis PRO* 1.171.39.46 (Rigaku OD, 2018), ShelXT (Sheldrick, 2015), *SHELXL* (Sheldrick, 2015), Olex2 (Dolomanov *et al.*, 2009).

Tables S5. Experimental details for compound **PFBP-2b_crystalB**

Crystal data	
Chemical formula	$C_{35}H_{30}F_9N$
M_r	635.60
Crystal system, space group	Triclinic, *P*-1
Temperature (K)	100
a, *b*, *c* (Å)	10.512 (4), 11.169 (4), 14.712 (4)
α, β, γ (°)	97.80 (3), 108.96 (3), 106.05 (3)
V (Å^3)	1520.8 (10)
Z	2
Radiation type	Mo *K*α
μ (mm^{-1})	0.12
Crystal size (mm)	0.38 × 0.18 × 0.05
Data collection	
Diffractometer	Xcalibur, Atlas
Absorption correction	Multi-scan *CrysAlis PRO* 1.171.38.46 (Rigaku Oxford Diffraction, 2015) Empirical absorption correction using spherical harmonics, implemented in SCALE3 ABSPACK scaling algorithm.
T_{min}, T_{max}	0.950, 1.000
No. of measured, independent and observed [$I > 2\sigma(I)$] reflections	27147, 7537, 5361

R_{int}	0.027
$(\sin \theta/\lambda)_{max}$ (Å^{-1})	0.694
Refinement	
$R[F^2 > 2\sigma(F^2)]$, $wR(F^2)$, S	0.043, 0.112, 1.02
No. of reflections	7537
No. of parameters	461
H-atom treatment	H-atom parameters constrained
$\Delta\rho_{max}$, $\Delta\rho_{min}$ (e Å^{-3})	0.33, −0.24

Computer programs: *CrysAlis PRO* 1.171.38.46 (Rigaku OD, 2015), ShelXT (Sheldrick, 2015), *SHELXL* (Sheldrick, 2015), Olex2 (Dolomanov *et al.*, 2009).

Rigaku Oxford Diffraction, CrysAlisPro Software System, Version 1.171, Rigaku Corporation, Oxford, UK, 2015.
Dolomanov, O. V., Bourhis, L. J., Gildea, R. J., Howard, J. A. K. & Puschmann, H. (2009). *J. Appl. Cryst.* **42**, 339–341.
Sheldrick, G. M. (2015). *Acta Cryst.* A**71**, 3–8.
Sheldrick, G. M. (2015). *Acta Cryst.* C**71**, 3–8.

References

(1) J. C. de Mello, H. F. Wittmann, R. H. Friend. *Adv. Mater*. 1997, **9**, 230–232.

(2) N. A. Kukhta, D. Volyniuk, L. Peciulyte, J. Ostrauskaite, G. Juska, J. V. Grazulevicius. *Dyes. Pigm*., 2015, **117**, 122–132.

(3) D. Gudeika, J. V. Grazulevicius, D. Volyniuk, G. Juska, V. Jankauskas, G. Sini. *J. Phys. Chem. C*, 2015, **119**, 28335−28346.

(4) G. Grybauskaite-Kaminskiene, D. Volyniuk, V. Mimaite, O. Bezvikonnyi, A. Bucinskas, G. Bagdziunas, J. V. Grazulevicius. *Chem. Eur.J.* 2018, **24**, 9581 –9591